S100A4 Protein Is Essential for the Development of Mature Microfold Cells in Peyer's Patches

國村, 和史

https://doi.org/10.15017/4059953

出版情報：九州大学, 2019, 博士（医学）, 課程博士
バージョン：

Article

Cell Reports

S100A4 Protein Is Essential for the Development of Mature Microfold Cells in Peyer's Patches

Graphical Abstract

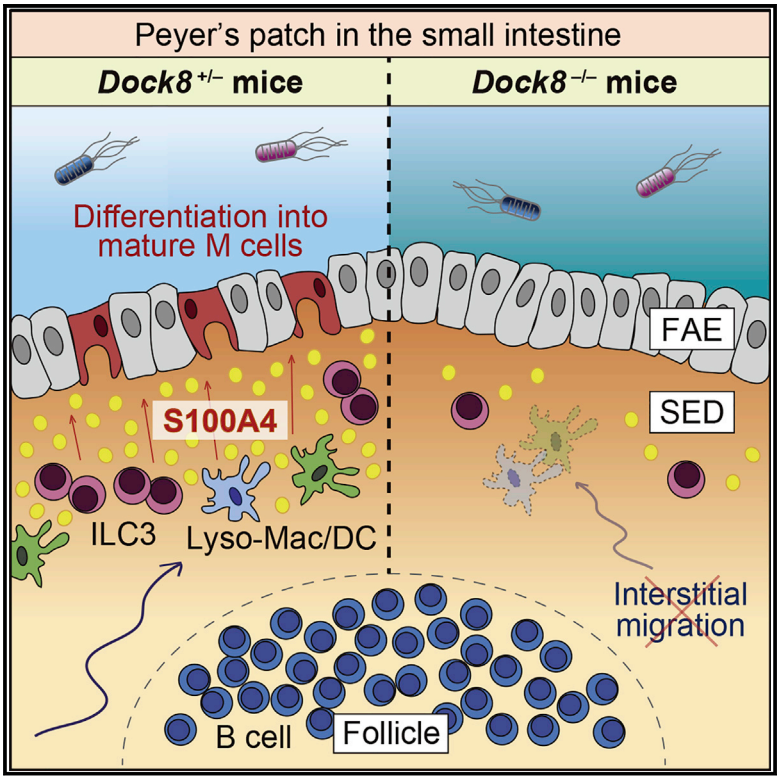

Highlights

- DOCK8 plays a key role in the development of mature M cells in Peyer's patches
- DOCK8 controls the localization of S100A4-producing cells in the subepithelial dome
- S100A4 protein promotes M cell maturation in organoid culture
- Deficiency of S100A4 prevents the development of mature M cells in mice

Authors

Kazufumi Kunimura, Daiji Sakata, Xin Tun, ..., Shouichi Ohga, Yasunobu Yoshikai, Yoshinori Fukui

Correspondence

fukui@bioreg.kyushu-u.ac.jp

In Brief

Kunimura et al. find that in the absence of DOCK8, S100A4-producing cells are reduced in the subepithelial dome, resulting in a maturation defect of M cells in Peyer's patches. *In vitro* and *in vivo* studies demonstrate that S100A4 protein is a key environmental factor that promotes M cell maturation.

Kunimura et al., 2019, Cell Reports *29*, 2823–2834
November 26, 2019
https://doi.org/10.1016/j.celrep.2019.10.091

CellPress

Cell Reports
Article

S100A4 Protein Is Essential for the Development of Mature Microfold Cells in Peyer's Patches

Kazufumi Kunimura,[1] Daiji Sakata,[1,2] Xin Tun,[3] Takehito Uruno,[1,2] Miho Ushijima,[1] Tomoya Katakai,[4] Akira Shiraishi,[5] Ryosuke Aihara,[1] Yasuhisa Kamikaseda,[1] Keisuke Matsubara,[1] Hirokazu Kanegane,[6] Shinichiro Sawa,[7] Gérard Eberl,[8] Shouichi Ohga,[5] Yasunobu Yoshikai,[3] and Yoshinori Fukui[1,2,9,*]

[1]Division of Immunogenetics, Department of Immunobiology and Neuroscience, Medical Institute of Bioregulation, Kyushu University, Fukuoka 812-8582, Japan
[2]Research Center for Advanced Immunology, Kyushu University, Fukuoka 812-8582, Japan
[3]Division of Host Defence, Medical Institute of Bioregulation, Kyushu University, Fukuoka 812-8582, Japan
[4]Department of Immunology, Niigata University Graduate School of Medical and Dental Sciences, Niigata 951-8510, Japan
[5]Department of Pediatrics, Graduate School of Medical Sciences, Kyushu University, Fukuoka 812-8582, Japan
[6]Department of Child Health and Development, Graduate School of Medical and Dental Sciences, Tokyo Medical and Dental University, Tokyo 113-8519, Japan
[7]Division of Mucosal Immunology, Research Center for Systems Immunology, Medical Institute of Bioregulation, Kyushu University, Fukuoka 812-8582, Japan
[8]Microenvironment & Immunity Unit, INSERM U1224, Institut Pasteur, Paris 75724, France
[9]Lead Contact
*Correspondence: fukui@bioreg.kyushu-u.ac.jp
https://doi.org/10.1016/j.celrep.2019.10.091

SUMMARY

Intestinal microfold cells (M cells) in Peyer's patches are a special subset of epithelial cells that initiate mucosal immune responses through uptake of luminal antigens. Although the cytokine receptor activator of nuclear factor-κB ligand (RANKL) expressed on mesenchymal cells triggers differentiation into M cells, other environmental cues remain unknown. Here, we show that the metastasis-promoting protein S100A4 is required for development of mature M cells. S100A4-producing cells are a heterogenous cell population including lysozyme-expressing dendritic cells and group 3 innate lymphoid cells. We found that in the absence of DOCK8, a Cdc42 activator critical for interstitial leukocyte migration, S100A4-producing cells are reduced in the subepithelial dome, resulting in a maturation defect of M cells. While S100A4 promotes differentiation into mature M cells in organoid culture, genetic inactivation of *S100a4* prevents the development of mature M cells in mice. Thus, S100A4 is a key environmental cue that regulates M cell differentiation in collaboration with RANKL.

INTRODUCTION

The mucosal surface of the intestinal tract is continuously exposed to a variety of foreign proteins and microorganisms. To induce antigen-specific immune responses against these antigens, the intestinal immune system has evolved unique lymphoid tissues called gut-associated lymphoid tissues (GALTs). Peyer's patches (PPs) are well-characterized GALTs in the small intestine (Mabbott et al., 2013) and are the main site for the induction of secretory immunoglobulin A (sIgA) (Cerutti and Rescigno, 2008; Pabst, 2012). PPs are composed of three functionally distinct areas: follicles containing a germinal center (GC), an interfollicular region (IFR) rich in T cells, and the subepithelial dome (SED), where IgA class switching is initiated (Cerutti and Rescigno, 2008; Mabbott et al., 2013; Pabst, 2012). Although PPs lack afferent lymphatics, PPs directly sample luminal antigens across the epithelial barrier via microfold (M) cells (Mabbott et al., 2013; Pabst, 2012), which are located in the follicle-associated epithelium (FAE) covering the PPs. M cells also express glycoprotein 2 (GP2) that contributes to uptake of *Salmonella* Typhimurium by recognizing the bacterial flagellar protein FimH (Hase et al., 2009; Mabbott et al., 2013; Terahara et al., 2008). It has been shown that the lack of M cells or GP2 impairs antigen-specific T cell responses in the PPs of mice orally infected with *Salmonella* Typhimurium (Hase et al., 2009). Thus, M-cell-mediated antigen sampling is an important step in the initiation of intestinal immune responses.

M cells arise from cycling intestinal crypt stem cells expressing Lgr5 (de Lau et al., 2012; Kanaya et al., 2018). Because of the restricted localization of M cells in the FAE, it has been postulated that additional signals from the stromal or immune cells in the SED are required to induce M cell differentiation. One of these signals is provided by receptor activator of nuclear factor-κB ligand (RANKL) (Mabbott et al., 2013). RANKL is a member of the tumor necrosis factor (TNF) family cytokine that transmits the signal through RANK expressed by epithelial cells. So far, deletion of RANK in epithelial cells has been shown to impair M cell development (Rios et al., 2016). Similarly, RANKL-deficient mice have very few M cells, but exogenous administration of recombinant RANKL restores the number of M cells in these mice (Knoop et al., 2009). This effect of RANKL is partly mediated by induction of the transcription factor Spi-B.

Indeed, GP2-positive mature M cells are absent in PPs from Spi-B-deficient mice, whereas Marcksl1^{+}AnnexinV^{+} immature M cells are intact (de Lau et al., 2012; Kanaya et al., 2012; Sato et al., 2013). RANKL is initially synthesized as a transmembrane protein and can be released from the cell surface following cleavage by metalloproteases. Recent evidence indicates that mesenchymal stromal cells designated M-cell inducer cells (MCi cells) in the SED express the membrane-bound RANKL and promote M cell development through the interaction with FAE (Nagashima et al., 2017). However, other environmental cues important for M cell development remain unknown.

DOCK8 is an evolutionarily conserved guanine nucleotide exchange factor (GEF) for Cdc42 (Harada et al., 2012), and its mutations in humans cause a combined immunodeficiency characterized by recurrent viral infections, early-onset malignancy, and atopic dermatitis (Engelhardt et al., 2015; Sanal et al., 2012; Zhang et al., 2009, 2010). Accumulating evidence indicates that human patients with *DOCK8* mutations have morphological and functional abnormalities of leukocytes (Jabara et al., 2012; Mizesko et al., 2013; Randall et al., 2011; Zhang et al., 2009, 2014). In addition, the important roles of DOCK8 in leukocytes have been demonstrated using animal models. For example, *N*-ethyl-*N*-nitrosourea-mediated mutagenesis in mice has shown that DOCK8 regulates immunological synapse formation in B cells and is required for development or survival of memory CD8^{+} T cells, natural killer T cells, and group 3 innate lymphoid cells (ILC3s) (Crawford et al., 2013; Lambe et al., 2011; Randall et al., 2009, 2011; Singh et al., 2014; Zhang et al., 2014). On the other hand, by generating DOCK8-deficient (*Dock8*$^{-/-}$) mice, we and others have revealed that DOCK8 is essential for interstitial migration of dendritic cells (DCs) (Harada et al., 2012; Krishnaswamy et al., 2015, 2017). Yet, the role of DOCK8 in mucosal immune responses is poorly understood.

S100A4 belongs to the S100 family of proteins that contain two Ca^{2+}-binding sites, including a canonical EF-hand motif (Schneider et al., 2008). Although *S100a4* was initially identified as a gene specifically expressed in metastatic tumor cell lines (Boye and Maelandsmo, 2010), S100A4 is expressed not only in tumor cells but also in normal cells, including leukocytes such as macrophages and DCs (Österreicher et al., 2011; Sun et al., 2017; Zhang et al., 2018). S100A4 has both intracellular and extracellular effects. Intracellularly, S100A4 interacts with cytoskeletal proteins and enhances metastasis of several types of tumor cells (Boye and Maelandsmo, 2010). In addition, S100A4 is secreted from both tumor and normal cells and exerts extracellular effects to promote angiogenesis, neurite outgrowth, and cell proliferation (Ambartsumian et al., 2001; Dmytriyeva et al., 2012; Klingelhöfer et al., 2009; Novitskaya et al., 2000). In this study, we found that in the absence of DOCK8, S100A4-producing cells were markedly reduced in the SED, resulting in a developmental defect of mature M cells. While soluble S100A4 promoted differentiation into mature M cells in intestinal organoid culture by activating a transcriptional program, genetic inactivation of *S100a4* prevented the development of mature M cells in mice. Our results thus identify S100A4 as a key environmental factor essential for the development of mature M cells.

RESULTS

Impaired Development of Mature M Cells in *Dock8*$^{-/-}$ Mice

It is known that DOCK8 is expressed in various tissues and cell types (Ruusala and Aspenström, 2004; Yamamura et al., 2017). Consistent with this, immunostaining of PPs revealed that DOCK8 is widely distributed in the follicle, SED, and FAE (Figures S1A and S1B). Although PPs were small and few in number in the case of conventional *Dock8*$^{-/-}$ mice, the overall architecture of PPs was normal even in the absence of DOCK8 (Figures S1C–S1F). To functionally examine the role of DOCK8 in intestinal immune responses, we orally immunized conventional *Dock8*$^{+/-}$ and *Dock8*$^{-/-}$ littermate mice with cholera toxin (CTX). When the feces and serum were taken from *Dock8*$^{+/-}$ mice 2 weeks after immunization, CTX-specific IgA antibody was readily detected in both samples (Figure 1A). However, CTX-specific IgA antibody production was impaired in the case of *Dock8*$^{-/-}$ mice (Figure 1A). Although antibody production involves a complex cascade of molecular and cellular interactions, an initial and important step is uptake of luminal antigens by M cells. As M cells are particularly important for the uptake of particulate antigens, we next compared the uptake of fluorescent particles (200 nm in diameter) between conventional *Dock8*$^{+/-}$ and *Dock8*$^{-/-}$ mice. In *Dock8*$^{+/-}$ mice, particles were abundantly found in the SED of PPs, whereas very few particles were taken up into the PPs of *Dock8*$^{-/-}$ mice (Figure 1B). More importantly, uptake of orally administered FimH^{+} *Salmonella enterica* serovar Choleraesuis (*S.* Choleraesuis) was markedly reduced in PPs of *Dock8*$^{-/-}$ mice as compared with that in *Dock8*$^{+/-}$ mice (Figure 1C). These findings led us to examine whether *Dock8*$^{-/-}$ mice have quantitative or qualitative defects in M cells. Indeed, whole -mount immunostaining of PPs revealed that the number of GP2^{+} mature M cells per field of FAE was markedly reduced in *Dock8*$^{-/-}$ mice as compared with that in *Dock8*$^{+/-}$ mice (Figure 1D). This was further confirmed by scanning electron microscopic analysis of PPs in *Dock8*$^{-/-}$ mice (Figure 1E). On the other hand, AnnexinV^{+} GP2^{-} immature M cells increased in PPs from *Dock8*$^{-/-}$ mice (Figure 1F). Collectively, these results indicate that DOCK8 plays a key role in differentiation of the phenotypically and functionally mature M cells.

M Cell Maturation Requires DOCK8 Expression in S100A4-Producing Cells

To identify the specific cell types that require DOCK8 expression for maturation of M cells, we developed the gene-targeted mice harboring *loxP*-flanked exon3 of *Dock8* allele (*Dock8*$^{lox/lox}$) (Figure S2A). First, we crossed them with *Vil1-Cre-ER*^{T2} mice (el Marjou et al., 2004) to see whether DOCK8 regulates M cell development in a cell-intrinsic manner. When tamoxifen was intraperitoneally injected into *Vil1-Cre-ER*^{T2} *Dock8*$^{lox/lox}$ mice for 5 days, DOCK8 expression was deleted in intestinal epithelial cells (Figure S2B), but GP2^{+} mature M cells were normally found in PPs of these mice (Figure 2A). Similarly, genetic deletion of DOCK8 in CD11c^{+} cells, lysozyme M^{+} cells, RORγt^{+} cells, or CD19^{+} cells alone did not affect M cell development (Figures 2B and S2C). Although RANKL presented by mesenchymal

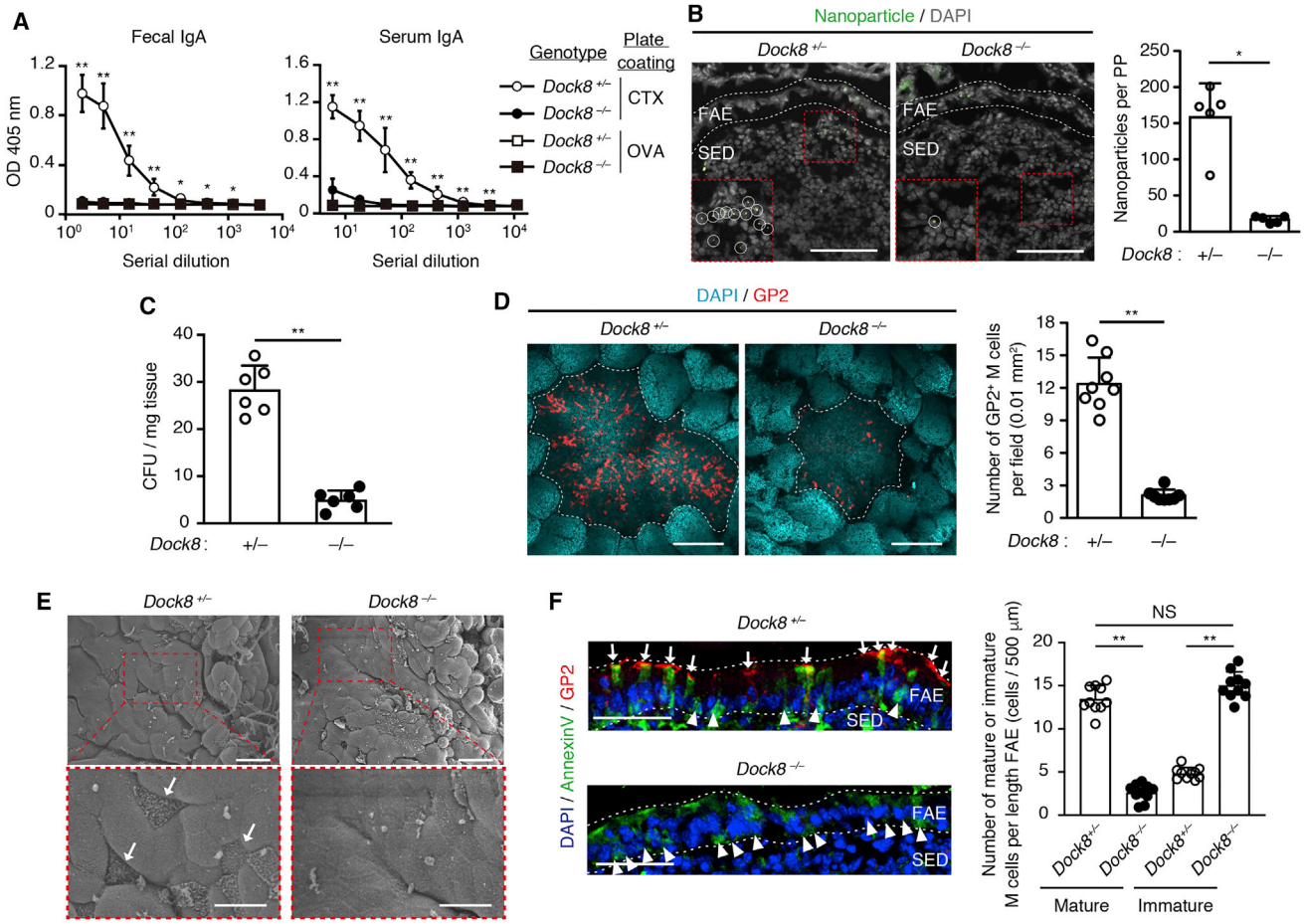

Figure 1. Impaired Development of Mature M Cells in *Dock8*$^{-/-}$ Mice

(A) Comparison of antigen-specific IgA antibody production between *Dock8*$^{+/-}$ and *Dock8*$^{-/-}$ mice at day 14 after oral immunization with CTX (n = 5). Ovalbumin (OVA) was used as a negative control.

(B) Uptake of fluorescent nanoparticles into PPs from *Dock8*$^{+/-}$ and *Dock8*$^{-/-}$ mice. The number of nanoparticles per PP was compared between them (n = 5). Higher magnifications of the indicated area are shown at the left corner. Scale bars, 50 μm.

(C) Uptake of *S.* Choleraesuis into PPs from *Dock8*$^{+/-}$ and *Dock8*$^{-/-}$ mice. The colonies of bacteria in the tissue homogenates of PPs were counted and are shown as colony-forming units (CFUs) (n = 6).

(D) Whole-mount immunostaining of PPs from *Dock8*$^{+/-}$ and *Dock8*$^{-/-}$ mice. The number of GP2^{+} M cells per field of FAE (0.01 mm^2) was compared between them (n = 8). Scale bars, 200 μm.

(E) Scanning electron microscopy of PPs from *Dock8*$^{+/-}$ and *Dock8*$^{-/-}$ mice. Higher magnifications (lower panels) of the area are outlined at upper panels. Arrows indicate M cells with short, sparse, and irregular microvilli. Scale bars, 20 μm (upper panels) and 10 μm (lower panels).

(F) Immunohistochemical analyses for AnnexinV and GP2 expression in PPs from *Dock8*$^{+/-}$ and *Dock8*$^{-/-}$ mice. The number of mature or immature M cells per length FAE (500 μm) was compared between them (n = 10). Arrows or arrowheads indicate AnnexinV^{+} GP2^{+} mature M cells or AnnexinV^{+} GP2^{-} immature M cells, respectively. Scale bars, 50 μm.

In (A)–(D) and (F), data are expressed as mean ± SD. *p < 0.05; **p < 0.01; NS, not significant by two-tailed Mann-Whitney test (A and B) and two-tailed unpaired Student's t test (C, D, and F).

See also Figure S1.

stromal cells (MCi cells) plays an important role in M cell development (Nagashima et al., 2017), expression of RANKL and distribution of MCi cells were unchanged between conventional *Dock8*$^{+/-}$ and *Dock8*$^{-/-}$ mice (Figures 2C and S2D). Consistent with this, M cell development occurred normally even when DOCK8 expression was deleted in MCi cells by crossing *Dock8*$^{lox/lox}$ mice with *Twist2-Cre* mice (Figures 2B and S2E), which specifically express *Cre* gene in mesenchymal cells (Geske et al., 2008).

Surprisingly, however, we found that the number of GP2^{+} mature M cells was markedly reduced when DOCK8 expression was deleted in S100A4-producing cells by crossing *Dock8*$^{lox/lox}$ mice with *S100a4-Cre* mice (Bhowmick et al., 2004) (Figures 3A, S3A, and S3B). As seen in conventional *Dock8*$^{-/-}$ mice (Figure 1A), *S100a4-Cre Dock8*$^{lox/lox}$ mice failed to produce an antigen-specific IgA antibody in the feces and serum when mice were orally immunized with CTX (Figure 3B). In addition, uptake of both orally administered particles and *S.* Choleraesuis were

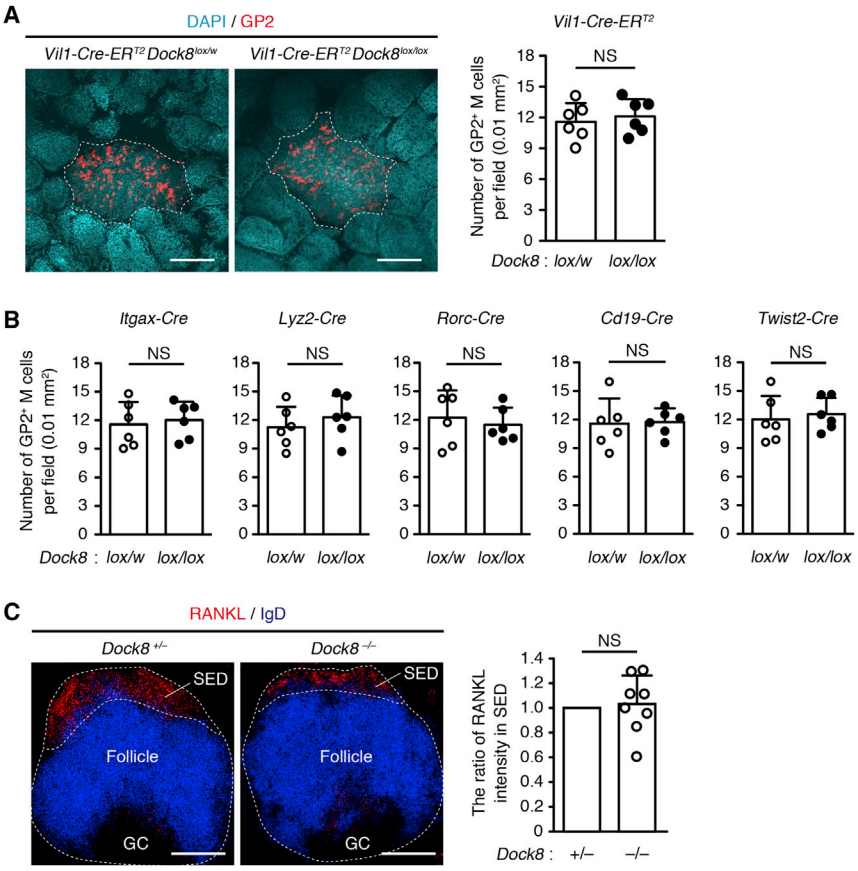

Figure 2. Effect of Cell-Type-Specific Deletion of DOCK8 on M Cell Differentiation

(A) Whole-mount immunostaining of PPs from *Vil1-Cre-ER^{T2} Dock8$^{lox/w}$* and *Dock8$^{lox/lox}$* mice. The number of GP2$^+$ M cells per field of FAE (0.01 mm^2) was compared between them (n = 6). Scale bars, 200 μm.

(B) The number of GP2$^+$ M cells per field of FAE (0.01 mm^2) in *Dock8$^{lox/w}$* and *Dock8$^{lox/lox}$* mice crossed with various cell-type specific *Cre* mice (n = 6 per each category of mice).

(C) Expression of RANKL in PPs from *Dock8$^{+/-}$* and *Dock8$^{-/-}$* mice. The fluorescence intensity of RANKL in the SED of *Dock8$^{-/-}$* mice to that in the *Dock8$^{+/-}$* SED is shown (n = 8). Scale bars, 200 μm.

In (A)–(C), data are expressed as mean ± SD. NS, not significant by two-tailed unpaired Student's t test.

See also Figure S2.

impaired in *S100a4-Cre Dock8$^{lox/lox}$* mice (Figures 3C and 3D). Thus, DOCK8 expression in S100A4-producing cells is critical for development of mature M cells. It has been reported that the relative abundance of segmented filamentous bacteria (SFB) in the gut microbiota increased in mice where M cell development is defective due to the lack of RANKL in MCi cells (Nagashima et al., 2017). In bacteria groups, SFB belongs to Clostridiales; Clostridiaceae (order; family). Similar results were obtained when fecal pellets from conventional *Dock8$^{-/-}$* mice and *S100a4-Cre Dock8$^{lox/lox}$* mice were analyzed by 16S rRNA sequencing (Figures 3E and 3F).

DOCK8 Deficiency Impairs Localization of S100A4-Producing Cells in the SED

Real-time PCR analyses showed that *S100a4* gene was abundantly expressed in PPs of wild-type (WT) C57BL/6 mice (Figure S4A). To visualize localization of S100A4-producing cells in PPs, we used transgenic mice expressing enhanced GFP under the control of the mouse *S100a4* promoter (S100A4-GFP mice) and crossed them with conventional *Dock8$^{-/-}$* mice. Immunofluorescence staining of PPs from WT and *Dock8$^{+/-}$* mice revealed that the majority of S100A4-producing cells (GFP$^+$ cells) were localized within the SED and IFR (Figures 4A and 4B). However, *Dock8$^{-/-}$* mice exhibited a severe reduction of S100A4-producing cells in the SED (Figure 4B). CD11c$^+$ mononuclear cells in the PPs are classified into conventional DCs and monocyte-derived lysozyme-expressing cells, designated Lyso-Mac and Lyso-DC (Bonnardel et al., 2015). Microarray analyses revealed that S100A4-producing cells expressed genes characteristic of Lyso-Mac/DCs (*Lyz2*, *Clec7a*, *Cx3cr1*, and *Cd209d*) and also those of ILC3s (*Il22* and *Rorc*) (Bonnardel et al., 2015; Colonna, 2018) (Figure 4C). This was confirmed by flow cytometric analyses showing that 16.7% and 12.7% of S100A4-producing cells were Lyso-Mac/DCs and ILC3 cells (Figures 4D and S4B), respectively. Interestingly, the number of GP2$^+$ mature M cells was significantly reduced in double-knockout mice (*Itgax-Cre Rorc-Cre Dock8$^{lox/lox}$* mice) where DOCK8 expression was deleted in both CD11c$^+$ cells and RORγt$^+$ cells (Figure 4E).

To further clarify whether Lyso-Mac/DCs and ILC3 cells can produce S100A4, we sorted Lyso-Mac/DCs (lysozyme-M-GFP$^+$ CD11c^{high} BST2$^+$) or ILC3 cells (RORγt-GFP$^+$ c-kit$^+$ Sca1$^-$ lineage$^-$) from PPs using transgenic mice expressing GFP under the control of the mouse *Lyz2* promoter (lysozyme-M-GFP mice) or *Rorc* promoter (RORγt-GFP mice), respectively. Indeed, these cells abundantly expressed *S100a4* gene compared with B cells and T cells (Figure S4C).

Although *Dock8$^{-/-}$* DCs migrate normally on two-dimensional surfaces, DOCK8 is required for DCs to pass through the narrow gaps of three-dimensional (3D) fibrillar networks (Harada et al., 2012; Krishnaswamy et al., 2015). As the SED area is rich in collagen fibers (Ohtani et al., 1991) (Figure S4D), a migration defect may underlie impaired accumulation of *Dock8$^{-/-}$* S100A4-producing cells in the SED. To address this possibility, we performed 3D migration assays using collagen gels. When *Dock8$^{+/-}$* Lyso-Mac/DCs were exposed to a diffusion gradient of CCL5, a chemokine highly expressed in the FAE of the PPs (Figure S4E generated from GSE93319 in Nagashima et al., 2017), they migrated efficiently toward the chemokine source (Figure 4F). However, the chemotactic response of *Dock8$^{-/-}$*

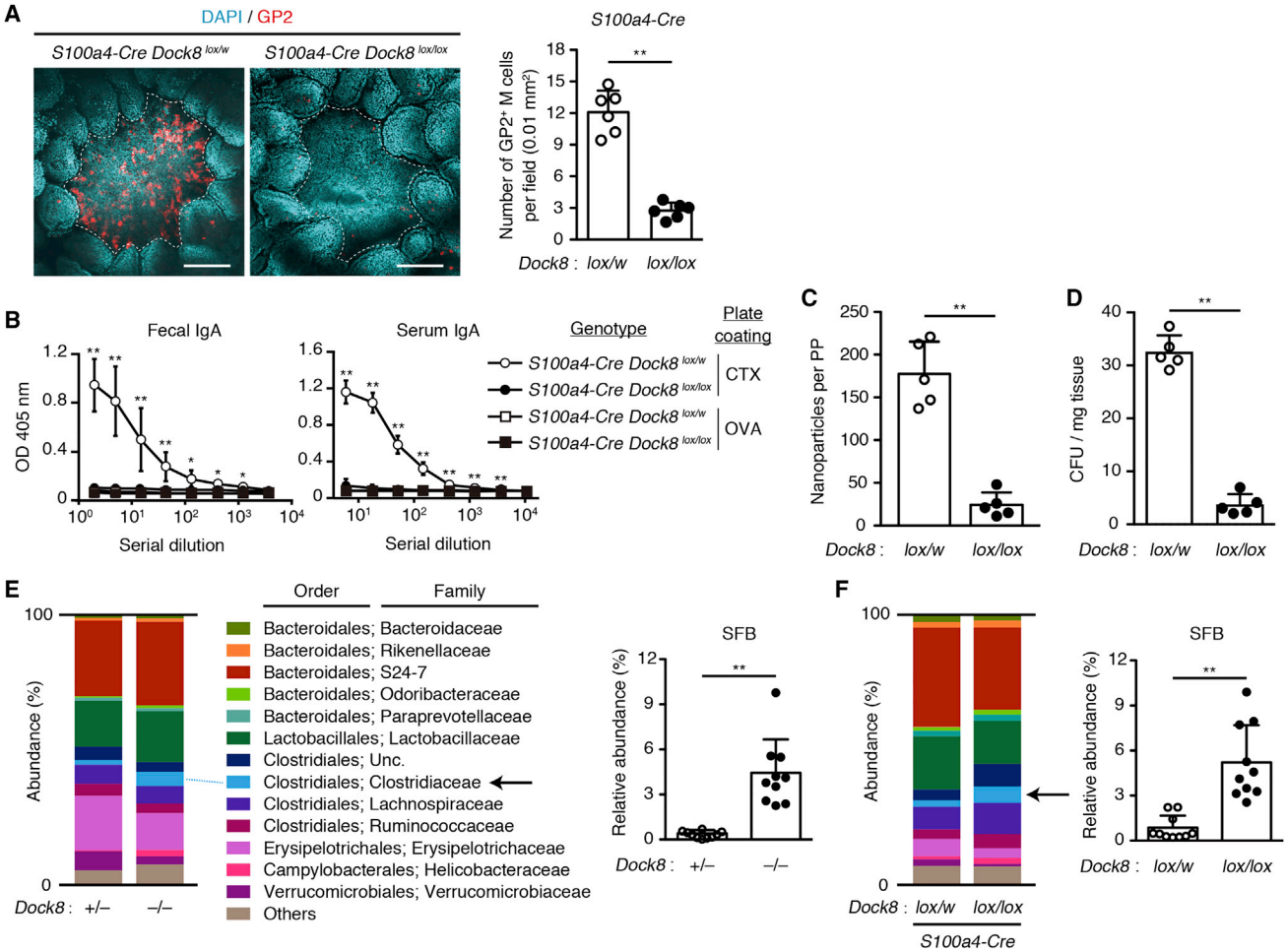

Figure 3. Impaired Development of Mature M Cells in *S100a4-Cre Dock8$^{lox/lox}$* Mice

(A) Whole-mount immunostaining of PPs from *S100a4-Cre Dock8$^{lox/w}$* and *Dock8$^{lox/lox}$* mice. The number of GP2$^+$ M cells per field of FAE (0.01 mm^2) was compared between them (n = 6). Scale bars, 200 μm.

(B) Comparison of CTX-specific IgA antibody production between *S100a4-Cre Dock8$^{lox/w}$* and *Dock8$^{lox/lox}$* mice at day 14 after oral immunization with CTX (n = 5). OVA was used as a negative control.

(C) Uptake of fluorescent nanoparticles into PPs from *S100a4-Cre Dock8$^{lox/w}$* and *Dock8$^{lox/lox}$* mice. The number of nanoparticles per PP was compared between them (n = 5).

(D) Uptake of *S.* Choleraesuis into PPs from *S100a4-Cre Dock8$^{lox/w}$* and *Dock8$^{lox/lox}$* mice. The colonies of bacteria in the tissue homogenates from PPs were counted and are shown as the CFU (n = 5).

(E and F) Relative abundance of the gut microbiota (major order; family) and abundance of 16S rRNA of SFB relative to the total bacteria in feces were compared between *Dock8$^{+/-}$* and *Dock8$^{-/-}$* mice (E; n = 10 fecal pellets from 10 mice) or between *S100a4-Cre Dock8$^{lox/w}$* and *Dock8$^{lox/lox}$* mice (F; n = 10 fecal pellets from 10 mice). Arrows indicate Clostridiales; Clostridiaceae to which SFB belongs.

In (A)–(F), data are expressed as mean ± SD. **p < 0.01 by two-tailed unpaired Student's t test (A and C–F) and two-tailed Mann-Whitney test (B).

See also Figure S3.

Lyso-Mac/DCs was severely impaired under the same experimental setting (Figure 4F). Similar results were obtained when chemotactic response to CX3CL1 was compared between *Dock8$^{+/-}$* Lyso-Mac/DCs and *Dock8$^{-/-}$* Lyso-Mac/DCs in collagen gels (Figure 4G).

S100A4 Promotes Differentiation into Mature M Cells in Organoid Culture

M cells can be differentiated *in vitro* from Lgr5$^+$ epithelial stem cells using intestinal organoid culture (de Lau et al., 2012; Kanaya et al., 2018). Although organoid formation requires defined factors such as epidermal growth factors (EGFs), R-spondin1, and Noggin, *Egf* gene is hardly expressed in WT PPs (Figure S4A). We found that without EGFs, crypts grew and formed organoid structure when intestinal crypts harboring stem cells were co-cultured with S100A4-GFP$^+$ or S100A4-GFP$^-$ cells (Figure 5A). However, the presence of S100A4-GFP$^+$ cells significantly augmented RANKL-induced expression of *Spib* and *Gp2* in organoids (Figure 5B). This effect of S100A4-GFP$^+$ cells was cancelled when anti-S100A4 antibody was added to the culture (Figure 5B), indicating that S100A4 protein itself is important for M cell differentiation. Indeed, the recombinant S100A4

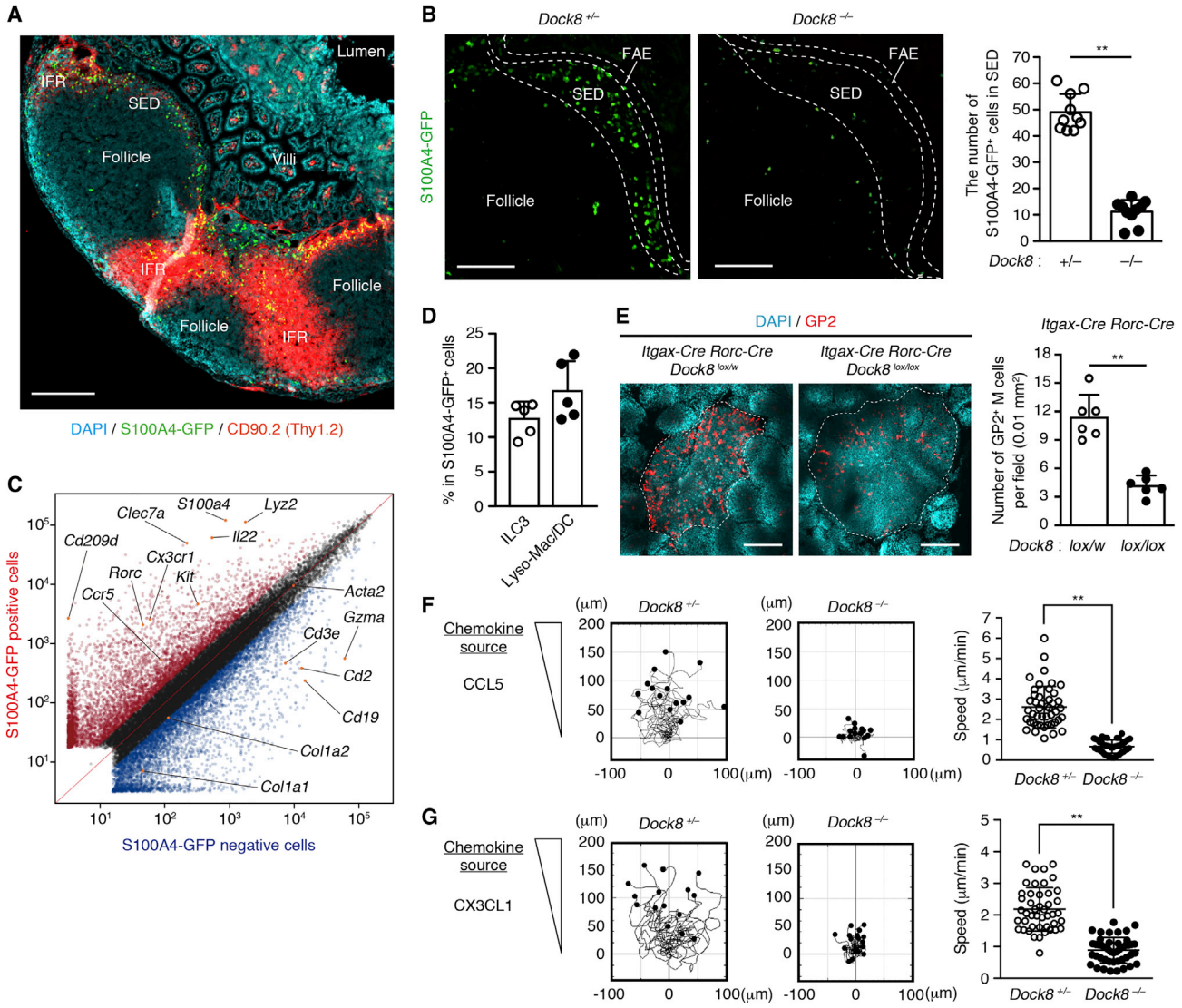

Figure 4. Localization and Characterization of S100A4-Producing Cells

(A) Visualization of S100A4-producing cells (S100A4-GFP$^+$ cells) in PPs using S100A4-GFP mice. Data are representative of three independent experiments. Scale bars, 200 μm.

(B) Localization of S100A4-producing cells (S100A4-GFP$^+$ cells) in PPs from *Dock8*$^{+/-}$ and *Dock8*$^{-/-}$ S100A4-GFP mice. The number of GFP$^+$ cells in the SED was compared between them (n = 10). Scale bars, 100 μm.

(C) Comparison of gene expression profiles between S100A4-GFP$^+$ cells (red) and S100A4-GFP$^-$ cells (blue). Cells were sorted from PPs pooled from five S100A4-GFP mice and used for microarray analysis.

(D) The percentage of ILC3 cells and Lyso-Mac/DCs to the total S100A4-producing cells (S100A4-GFP$^+$ cells) in PPs from S100A4-GFP mice (n = 5).

(E) Whole-mount immunostaining of PPs from *Itgax-Cre Rorc-Cre Dock8*$^{lox/w}$ and *Dock8*$^{lox/lox}$ mice. The number of GP2$^+$ M cells per field of FAE (0.01 mm^2) was compared between them (n = 6). Scale bars, 200 μm.

(F and G) Chemotactic responses of Lyso-Mac/DCs from *Dock8*$^{+/-}$ and *Dock8*$^{-/-}$ mice toward CCL5 (F) or CX3CL1 (G) in collagen gels (n = 45). Before assays, the lysozyme-M-GFP$^+$ CD11c^{high} BST2$^+$ cells were prepared from *Dock8*$^{+/-}$ and *Dock8*$^{-/-}$ lysozyme-M-GFP mice.

In (B) and (E)–(G), data are expressed as mean ± SD. **p < 0.01 by two-tailed unpaired Student's t test.

See also Figure S4.

protein, when used with RANKL, markedly increased the expression of *Spib* and *Gp2* in the organoids, as compared with the samples treated with RANKL alone (Figure 5C). Consistent with this, intestinal crypts from both *Dock8*$^{+/-}$ and *Dock8*$^{-/-}$ mice efficiently differentiated into GP2$^+$ mature M cells when cultured in the medium containing both S100A4 and RANKL (Figure 5D). Treatment with S100A4 protein also induced the expression of the Spi-B-dependent genes *Ccl9* and *Tnfaip2* in organoids (Figure 5E). On the other hand, treatment with S100A4 did not affect the expression of *Marcksl1* and *Anxa5*, which are expressed in

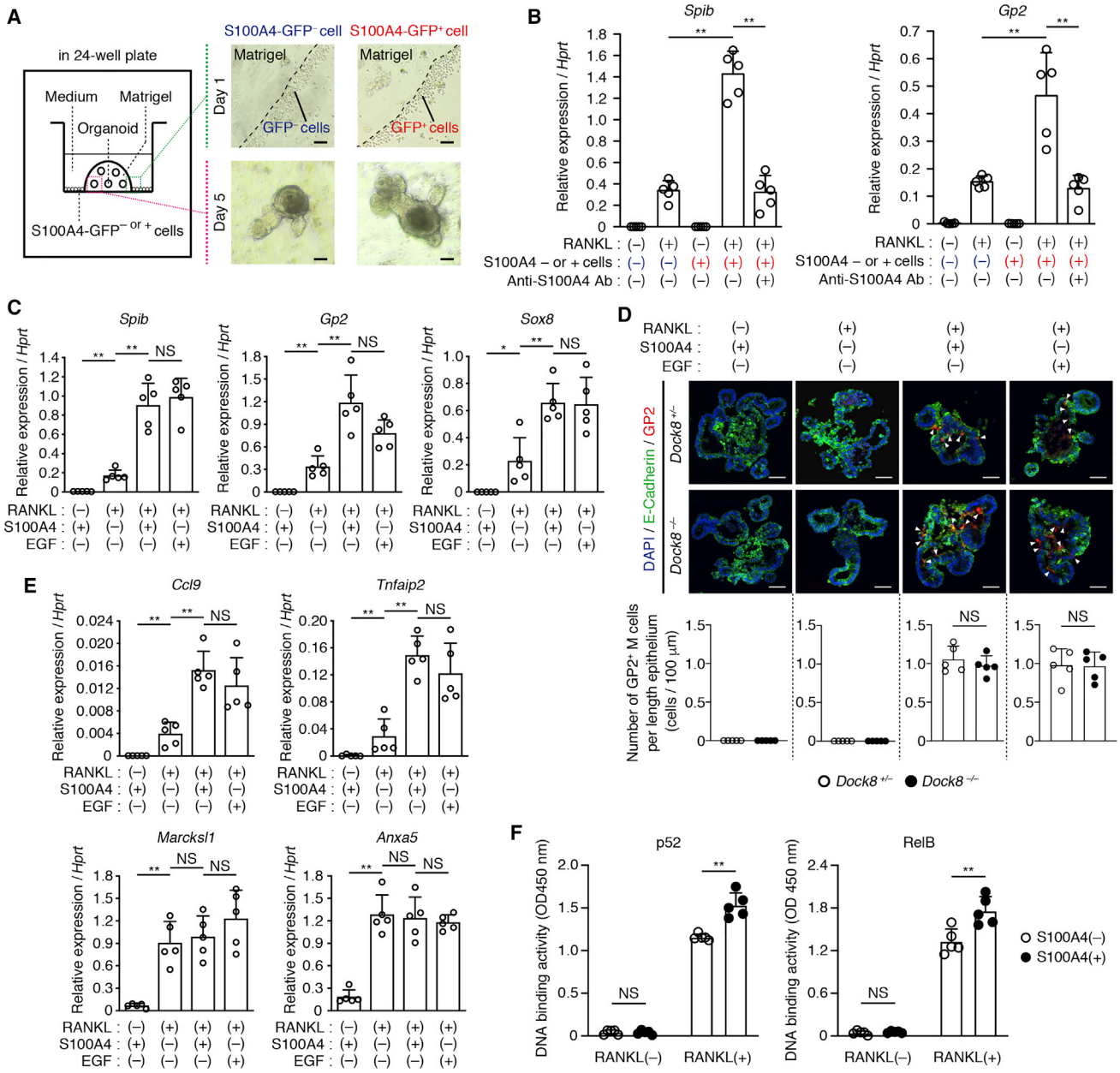

Figure 5. Effect of S100A4 on Development of Mature M Cells in Organoid Culture

(A) Schematic representation of the intestinal organoid culture used in this study and the actual images. Data are representative of three independent experiments. Scale bar, 50 μm.

(B) Expression of *Spib* and *Gp2* in the organoids generated from WT mice with S100A4-GFP$^+$ or S100A4-GFP$^-$ cells in the presence or absence of RANKL and anti-S100A4 antibody. Data (n = 5) were normalized with *Hprt* expression.

(C) Expression of *Spib*, *Gp2*, and *Sox8* in the organoids generated from WT mice in the presence of RANKL, S100A4, and/or EGF. Data (n = 5) were normalized with *Hprt* expression.

(D) Immunohistochemical analyses for GP2 and E-cadherin expression in the organoids generated from *Dock8*$^{+/-}$ or *Dock8*$^{-/-}$ mice in the presence of RANKL, S100A4, and/or EGF. The number of Gp2$^+$ M cells per length epithelium of organoids was compared between *Dock8*$^{+/-}$ and *Dock8*$^{-/-}$ mice (n = 5). Images are representative of three independent experiments. Scale bars, 50 μm.

(E) Expression of genes characteristic for mature (*Ccl9* and *Tnfaip2*) or immature (*Marcksl1* and *Anxa5*) M cells in the organoids generated from WT mice in the presence of RANKL, S100A4 and/or EGF. Data (n = 5) were normalized with *Hprt* expression.

(F) RANKL-induced activation of nuclear p52 and RelB in the organoids generated from WT mice in the presence or absence of S100A4 (n = 5).

In (B)–(F), data are expressed as mean ± SD. *p < 0.05; **p < 0.01; NS, not significant by one-way ANOVA with Tukey's multiple-comparison test (B, C, and E), two-tailed unpaired Student's t test (D), and two-way ANOVA with Tukey's multiple-comparison test (F).

See also Figure S5.

immature M cells independently of Spi-B (Kanaya et al., 2012) (Figure 5E).

Recently, it has been shown that Sox8, a member of the SRY-related high-mobility group (HMG) box transcription factors, is specifically expressed in M cells via RANKL-RelB signaling and induces *Gp2* expression by directly binding to its promoter (Kimura et al., 2019). As the recombinant S100A4 protein augmented RANKL-mediated p52/RelB activation and induced Sox8 expression in the organoids (Figures 5C and 5F), it is likely that the S100A4-RelB-Sox8 axis operates in promoting M cell maturation. On the other hand, recent studies indicate that S100A4 acts through ErbB receptors, including epidermal growth factor receptor (EGFR) (Cho et al., 2016; Klingelhöfer et al., 2009; Pankratova et al., 2018). We also found that S100A4-mediated gene expression of *Spib* and *Gp2* in organoids was suppressed in the presence of AG1478 or AG879, an inhibitor for ErbB1 or ErbB2, respectively (Figure S5A). Similarly, the effect of S100A4 was cancelled when anti-EGFR antibody was added to the culture (Figure S5B), suggesting that S100A4 acts, at least in part, through EGFR.

Impaired Development of Mature M Cells in S100A4-Deficient Mice

To examine the role of S100A4 in M cell development under more physiological conditions, we developed S100A4-deficient mice by using the CRISPR/Cas9 nuclease system (Figures 6A and S6). Although $GP2^+$ M cells were observed in $S100a4^{+/+}$ mice at a frequency of 12.0 per 0.01 mm^2 FAE, $GP2^+$ mature M cells were hardly detected in $S100a4^{-/-}$ mice (Figure 6B). On the other hand, S100A4 deficiency did not impair the development of $AnnexinV^+$ $GP2^-$ immature M cells (Figure 6C). Functionally, $S100a4^{-/-}$ mice failed to produce antigen-specific IgA antibody in the feces and serum when mice were orally immunized with CTX (Figure 6D). Uptake of both orally administered particles and *S.* Choleraesuis were impaired in $S100a4^{-/-}$ mice (Figures 6E and 6F). These results indicate that S100A4 is essential for development of mature M cells. Interestingly, the relative abundance of SFB in the microbiota also increased in $S100a4^{-/-}$ mice (Figure 6G), as seen in $Dock8^{-/-}$ mice and *S100a4-Cre* $Dock8^{lox/lox}$ mice (Figures 3E and 3F). We also found that in mice heterozygous for the mutant allele ($S100a4^{+/-}$), the number of M cells was reduced to 48% of that of the $S100a4^{+/+}$ mice (Figure 6B). As this reduction was well correlated with the amount of S100A4 protein (Figure 6A), a gene dosage effect is likely to operate in controlling S100A4-mediated M cell differentiation.

DISCUSSION

M cells are a special subset of intestinal epithelial cells that mediate uptake of luminal antigens to initiate mucosal immune responses (Mabbott et al., 2013; Pabst, 2012). Differentiation into M cells requires the membrane-bound RANKL presented by mesenchymal stromal cells (Nagashima et al., 2017). However, other factors controlling M cell development are poorly understood. Here, we have identified S100A4 protein as a key environmental cue essential for development of mature M cells. Although S100A4 did not affect the expression of *Marcksl1* and *Anxa5* that are characteristic of immature M cells, S100A4 promoted differentiation into $GP2^+$ mature M cells in organoid culture by activating a transcriptional program. Conversely, genetic inactivation of *S100a4* prevented the development of mature M cells in mice. Collectively, these results indicate that S100A4 critically regulates differentiation into mature M cells in collaboration with RANKL.

Although signaling of extracellular S100A4 was largely unexplored, resent studies indicate that S100A4 acts through ErbB receptors (Cho et al., 2016; Klingelhöfer et al., 2009; Pankratova et al., 2018). Among them, ErbB1 and ErbB2 are expressed abundantly by the FAE (GSE93319 in Nagashima et al., 2017). We found that both anti-EGFR antibody and the inhibitor for ErbB1/2 significantly suppressed S100A4-mediated gene expression of *Spib* and *Gp2* in organoids. These results suggest S100A4 acts, at least in part, through EGFR. The precise mechanism by which S100A4 promotes M cell differentiation remains to be determined. However, we have shown that treatment of organoids with S100A4 protein augmented RANKL-mediated p52/RelB activation and induced *Sox8*, a transcription factor that mediates the induction of *Gp2* expression in M cells by directly binding to its promoter. Therefore, it is likely that the S100A4-RelB-Sox8 axis operates in promoting M cell maturation.

In the small intestine, M cells are mostly confined to the FAE covering PPs. As both dome-associated crypts and villous crypts contain $Lgr5^+$ stem cells, it is conceivable that additional signals required for M cell differentiation would be provided from the cells beneath the FAE (Mabbott et al., 2013). In this study, we have shown that S100A4-producing cells are mainly localized within the SED under the steady state. It is clear that this localization is functionally important, because differentiation into mature M cells was impaired in $Dock8^{-/-}$ mice, where the number of S100A4-producing cells was markedly reduced in the SED. S100A4-producing cells are a heterogenous cell population including Lyso-Mac/DCs and ILC3 cells. We found that the chemotactic response of Lyso-Mac/DCs in collagen gels was severely impaired in the absence of DOCK8. As the SED area is rich in collagen fibers (Ohtani et al., 1991), this migration defect would explain impaired accumulation of S100A4-producing cells in the SED region in $Dock8^{-/-}$ mice.

Homozygous and compound heterozygous mutations in *DOCK8* in humans cause a combined immunodeficiency with multiple clinical complications. Among them, it has been reported that 12% of the patients are affected by gastrointestinal tract infections, including *Salmonella enteritis* (Sanal et al., 2012; Zhang et al., 2009). We found that differentiation into $GP2^+$ mature M cells is severely impaired in the absence of DOCK8. As GP2 acts for uptake of $FimH^+$ bacteria, including *Salmonella*, to initiate mucosal immune responses (Hase et al., 2009), there is a possibility that defective M cell development contributes to the increased susceptibility of DOCK8-deficient patients to gastrointestinal tract infections. In addition, we have shown that DOCK8 deficiency in mice causes an increase in SFB in the gut microbiota, which are known to expand in the absence of the effective IgA responses (Suzuki et al., 2004)

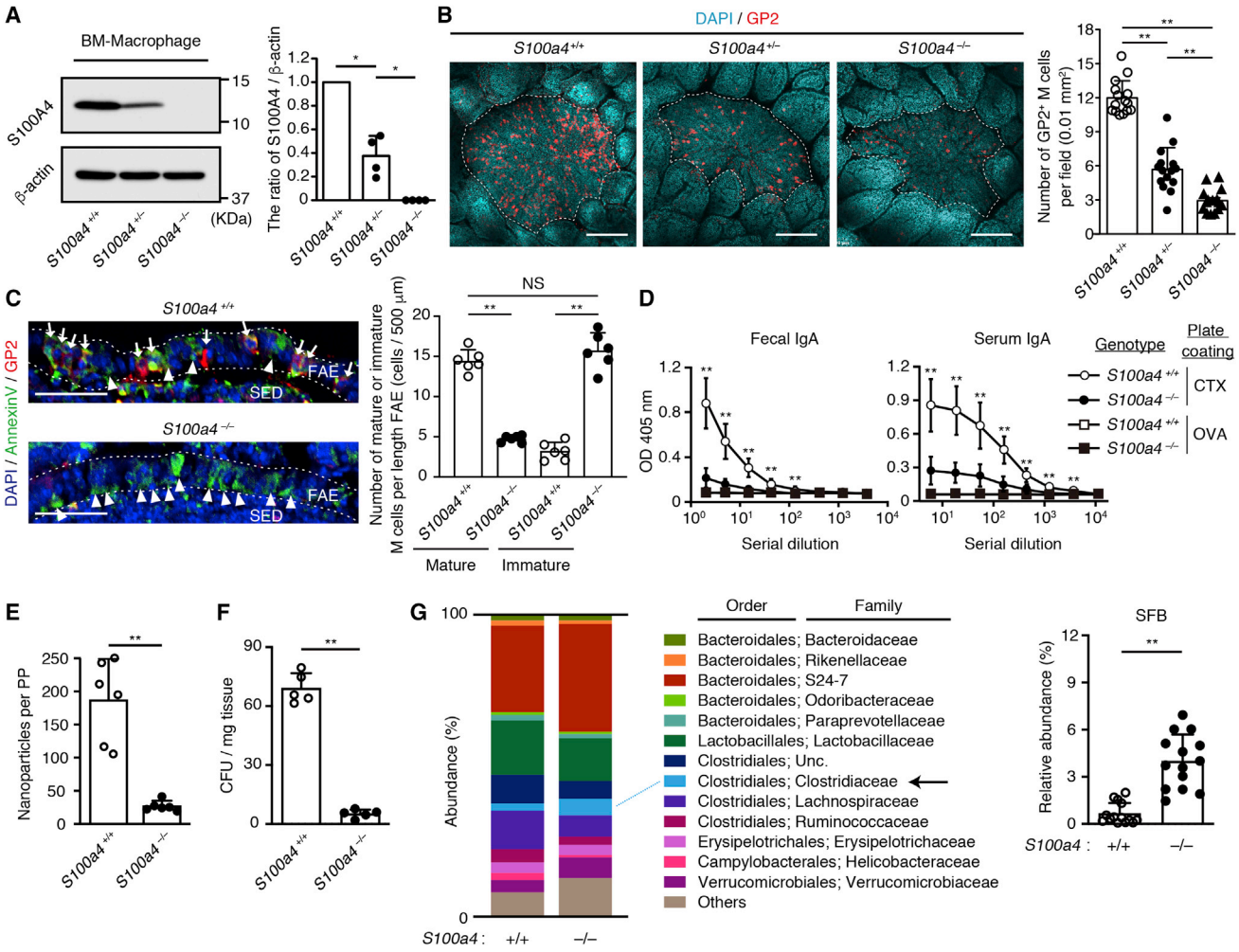

Figure 6. Impaired Development of Mature M Cells in *S100a4*$^{-/-}$ Mice

(A) Immunoblot showing S100A4 expression in bone marrow (BM)-derived macrophages from *S100A4*$^{+/+}$, *S100A4*$^{+/-}$, and *S100A4*$^{-/-}$ mice and their quantitative comparison (n = 4). Data are representative of four independent experiments. The expression of S100A4 relative to that of actin was normalized by setting the value of *S100A4*$^{+/+}$ sample as 1.

(B) Whole-mount immunostaining of PPs from *S100A4*$^{+/+}$, *S100A4*$^{+/-}$, and *S100A4*$^{-/-}$ mice. The number of GP2^{+} M cells per field of FAE (0.01 mm^2) was compared between them (n = 15). Scale bars, 200 μm.

(C) Immunohistochemical analyses for AnnexinV and GP2 expression in PPs from *S100a4*$^{+/+}$ and *S100a4*$^{-/-}$ mice. The number of mature and immature M cells per length FAE (500 μm) was compared between them (n = 6). Arrows or arrowheads indicate AnnexinV^{+} GP2^{+} mature M cells or AnnexinV^{+} GP2^{-} immature M cells, respectively. Scale bars, 50 μm.

(D) Comparison of CTX-specific IgA antibody production between *S100A4*$^{+/+}$ and *S100A4*$^{-/-}$ mice at day 14 after oral immunization with CTX (n = 5). OVA was used as a negative control.

(E) Uptake of fluorescent nanoparticles in PPs from *S100A4*$^{+/+}$ and *S100A4*$^{-/-}$ mice. The number of nanoparticles per PP was compared between them (n = 6).

(F) Uptake of *S.* Choleraesuis into PPs from *S100A4*$^{+/+}$ and *S100A4*$^{-/-}$ mice. The colonies of bacteria in the tissue homogenates of PPs were counted and are shown as CFUs (n = 5).

(G) Relative abundance of the gut microbiota (major order; family) and abundance of 16S rRNA of SFB relative to the total bacteria in feces were compared between *S100a4*$^{+/+}$ and *S100a4*$^{-/-}$ mice (n = 14 fecal pellets from 7 mice). Arrows indicate Clostridiales; Clostridiaceae to which SFB belongs.

In (A)–(G), data are expressed as mean ± SD. *p < 0.05; **p < 0.01; NS, not significant by two-tailed Mann-Whitney test (A, D, and G), one-way ANOVA with Tukey's multiple-comparison test (B), and two-tailed unpaired Student's t test (C, E, and F).

See also Figure S6.

and induce local and systemic inflammatory responses (Ivanov et al., 2009). Although further analyses are required, the altered composition of the gut microbiota may be involved in clinical complications associated with DOCK8 deficiency in humans.

In conclusion, we have identified S100A4 as a key environmental cue essential for development of mature M cells. Our findings thus define a previously unknown regulatory mechanism controlling M cell differentiation.

STAR★METHODS

Detailed methods are provided in the online version of this paper and include the following:

- KEY RESOURCES TABLE
- LEAD CONTACT AND MATERIALS AVAILABILITY
- EXPERIMENTAL MODEL AND SUBJECT DETAILS
  - Animals
  - Bacterial Strains
- METHOD DETAILS
  - Oral Immunization and ELISA
  - Uptake of Orally Administered Particles and Bacteria by M Cells
  - Whole Mount Immunostaining
  - Immunohistochemistry
  - Scanning Electron Microscopy
  - Isolation of Cells from Mouse Tissues
  - BM-Derived Macrophage Culture
  - Immunoblotting
  - Intestinal Organoid Culture
  - Flow Cytometry and Cell Sorting
  - 3D Chemotaxis Assay
  - ELISA for Measuring NFκB Activation
  - Reverse Transcription-PCR
  - Microarray Analysis
  - 16S rRNA Gene Sequencing
- QUANTIFICATION AND STATISTICAL ANALYSIS
- DATA AND CODE AVAILABILITY

SUPPLEMENTAL INFORMATION

Supplemental Information can be found online at https://doi.org/10.1016/j.celrep.2019.10.091.

ACKNOWLEDGMENTS

We thank Kei-ichi Nakayama (Kyushu University), Kiyoshi Takeda (Osaka University), Akira Suzuki (Kobe University), and Masaru Ishii (Osaka University) for providing genetically engineered mice. We thank Ayumi Inayoshi, Arisa Aosaka, Nao Kanematsu, Sayaka Akiyoshi, and Satomi Hori for technical assistance. This research was supported by the Leading Advanced Projects for Medical Innovation (LEAP JP19gm0010001 to Y.F.), Core Research for Evolutionary Medical Science and Technology (CREST JP19gm1310005 to Y.F.), and the Practical Research Project for Allergic Diseases and Immunology (JP19ek0410064 to Y.F.) from the Japan Agency for Medical Research and Development (AMED).

AUTHOR CONTRIBUTIONS

K.K., D.S., T.U., M.U., T.K., A.S., R.A., Y.K., and K.M. performed functional, histological, and biochemical analyses; X.T. and Y.Y. performed infection experiments; H.K., S.S., G.E., and S.O. provided clinical information or valuable reagents; K.K., T.U., H.K., S.S., G.E., S.O., and Y.F. contributed to writing the manuscript; Y.F. conceived the project, interpreted the data, and wrote the manuscript.

DECLARATION OF INTERESTS

The authors declare no competing interests.

Received: May 15, 2019
Revised: September 20, 2019
Accepted: October 22, 2019
Published: November 26, 2019

REFERENCES

Ambartsumian, N., Klingelhöfer, J., Grigorian, M., Christensen, C., Kriajevska, M., Tulchinsky, E., Georgiev, G., Berezin, V., Bock, E., Rygaard, J., et al. (2001). The metastasis-associated Mts1(S100A4) protein could act as an angiogenic factor. Oncogene *20*, 4685–4695.

Bhowmick, N.A., Chytil, A., Plieth, D., Gorska, A.E., Dumont, N., Shappell, S., Washington, M.K., Neilson, E.G., and Moses, H.L. (2004). TGF-β signaling in fibroblasts modulates the oncogenic potential of adjacent epithelia. Science *303*, 848–851.

Bonnardel, J., Da Silva, C., Henri, S., Tamoutounour, S., Chasson, L., Montañana-Sanchis, F., Gorvel, J.P., and Lelouard, H. (2015). Innate and adaptive immune functions of peyer's patch monocyte-derived cells. Cell Rep. *11*, 770–784.

Boye, K., and Maelandsmo, G.M. (2010). S100A4 and metastasis: a small actor playing many roles. Am. J. Pathol. *176*, 528–535.

Caton, M.L., Smith-Raska, M.R., and Reizis, B. (2007). Notch-RBP-J signaling controls the homeostasis of CD8⁻ dendritic cells in the spleen. J. Exp. Med. *204*, 1653–1664.

Cerutti, A., and Rescigno, M. (2008). The biology of intestinal immunoglobulin A responses. Immunity *28*, 740–750.

Cho, C.C., Chou, R.-H., and Yu, C. (2016). Amlexanox blocks the interaction between S100A4 and epidermal growth factor and inhibits cell proliferation. PLoS ONE *11*, e0161663.

Clausen, B.E., Burkhardt, C., Reith, W., Renkawitz, R., and Förster, I. (1999). Conditional gene targeting in macrophages and granulocytes using LysMcre mice. Transgenic Res. *8*, 265–277.

Colonna, M. (2018). Innate lymphoid cells: diversity, plasticity, and unique functions in immunity. Immunity *48*, 1104–1117.

Cong, L., Ran, F.A., Cox, D., Lin, S., Barretto, R., Habib, N., Hsu, P.D., Wu, X., Jiang, W., Marraffini, L.A., and Zhang, F. (2013). Multiplex genome engineering using CRISPR/Cas systems. Science *339*, 819–823.

Crawford, G., Enders, A., Gileadi, U., Stankovic, S., Zhang, Q., Lambe, T., Crockford, T.L., Lockstone, H.E., Freeman, A., Arkwright, P.D., et al. (2013). DOCK8 is critical for the survival and function of NKT cells. Blood *122*, 2052–2061.

de Lau, W., Kujala, P., Schneeberger, K., Middendorp, S., Li, V.S., Barker, N., Martens, A., Hofhuis, F., DeKoter, R.P., Peters, P.J., et al. (2012). Peyer's patch M cells derived from Lgr5(+) stem cells require SpiB and are induced by RankL in cultured "miniguts". Mol. Cell. Biol. *32*, 3639–3647.

Dmytriyeva, O., Pankratova, S., Owczarek, S., Sonn, K., Soroka, V., Ridley, C.M., Marsolais, A., Lopez-Hoyos, M., Ambartsumian, N., Lukanidin, E., et al. (2012). The metastasis-promoting S100A4 protein confers neuroprotection in brain injury. Nat. Commun. *3*, 1197.

el Marjou, F., Janssen, K.P., Chang, B.H., Li, M., Hindie, V., Chan, L., Louvard, D., Chambon, P., Metzger, D., and Robine, S. (2004). Tissue-specific and inducible Cre-mediated recombination in the gut epithelium. Genesis *39*, 186–193.

Engelhardt, K.R., Gertz, M.E., Keles, S., Schäffer, A.A., Sigmund, E.C., Glocker, C., Saghafi, S., Pourpak, Z., Ceja, R., Sassi, A., et al. (2015). The extended clinical phenotype of 64 patients with dedicator of cytokinesis 8 deficiency. J. Allergy Clin. Immunol. *136*, 402–412.

Faust, N., Varas, F., Kelly, L.M., Heck, S., and Graf, T. (2000). Insertion of enhanced green fluorescent protein into the lysozyme gene creates mice with green fluorescent granulocytes and macrophages. Blood *96*, 719–726.

Geske, M.J., Zhang, X., Patel, K.K., Ornitz, D.M., and Stappenbeck, T.S. (2008). Fgf9 signaling regulates small intestinal elongation and mesenchymal development. Development *135*, 2959–2968.

Harada, Y., Tanaka, Y., Terasawa, M., Pieczyk, M., Habiro, K., Katakai, T., Hanawa-Suetsugu, K., Kukimoto-Niino, M., Nishizaki, T., Shirouzu, M., et al. (2012). DOCK8 is a Cdc42 activator critical for interstitial dendritic cell migration during immune responses. Blood *119*, 4451–4461.

Hase, K., Kawano, K., Nochi, T., Pontes, G.S., Fukuda, S., Ebisawa, M., Kadokura, K., Tobe, T., Fujimura, Y., Kawano, S., et al. (2009). Uptake through glycoprotein 2 of FimH(+) bacteria by M cells initiates mucosal immune response. Nature *462*, 226–230.

Ivanov, I.I., Atarashi, K., Manel, N., Brodie, E.L., Shima, T., Karaoz, U., Wei, D., Goldfarb, K.C., Santee, C.A., Lynch, S.V., et al. (2009). Induction of intestinal Th17 cells by segmented filamentous bacteria. Cell *139*, 485–498.

Iwano, M., Plieth, D., Danoff, T.M., Xue, C., Okada, H., and Neilson, E.G. (2002). Evidence that fibroblasts derive from epithelium during tissue fibrosis. J. Clin. Invest. *110*, 341–350.

Jabara, H.H., McDonald, D.R., Janssen, E., Massaad, M.J., Ramesh, N., Borzutzky, A., Rauter, I., Benson, H., Schneider, L., Baxi, S., et al. (2012). DOCK8 functions as an adaptor that links TLR-MyD88 signaling to B cell activation. Nat. Immunol. *13*, 612–620.

Kanaya, T., Hase, K., Takahashi, D., Fukuda, S., Hoshino, K., Sasaki, I., Hemmi, H., Knoop, K.A., Kumar, N., Sato, M., et al. (2012). The Ets transcription factor Spi-B is essential for the differentiation of intestinal microfold cells. Nat. Immunol. *13*, 729–736.

Kanaya, T., Sakakibara, S., Jinnohara, T., Hachisuka, M., Tachibana, N., Hidano, S., Kobayashi, T., Kimura, S., Iwanaga, T., Nakagawa, T., et al. (2018). Development of intestinal M cells and follicle-associated epithelium is regulated by TRAF6-mediated NF-κB signaling. J. Exp. Med. *215*, 501–519.

Kawahara, K., Haraguchi, Y., Tsuchimoto, M., Terakado, N., and Danbara, H. (1988). Evidence of correlation between 50-kilobase plasmid of *Salmonella choleraesuis* and its virulence. Microb. Pathog. *4*, 155–163.

Kimura, S., Kobayashi, N., Nakamura, Y., Kanaya, T., Takahashi, D., Fujiki, R., Mutoh, M., Obata, Y., Iwanaga, T., Nakagawa, T., et al. (2019). Sox8 is essential for M cell maturation to accelerate IgA response at the early stage after weaning in mice. J. Exp. Med. *216*, 831–846.

Klingelhöfer, J., Møller, H.D., Sumer, E.U., Berg, C.H., Poulsen, M., Kiryushko, D., Soroka, V., Ambartsumian, N., Grigorian, M., and Lukanidin, E.M. (2009). Epidermal growth factor receptor ligands as new extracellular targets for the metastasis-promoting S100A4 protein. FEBS J. *276*, 5936–5948.

Knoop, K.A., Kumar, N., Butler, B.R., Sakthivel, S.K., Taylor, R.T., Nochi, T., Akiba, H., Yagita, H., Kiyono, H., and Williams, I.R. (2009). RANKL is necessary and sufficient to initiate development of antigen-sampling M cells in the intestinal epithelium. J. Immunol. *183*, 5738–5747.

Krishnaswamy, J.K., Singh, A., Gowthaman, U., Wu, R., Gorrepati, P., Sales Nascimento, M., Gallman, A., Liu, D., Rhebergen, A.M., Calabro, S., et al. (2015). Coincidental loss of DOCK8 function in NLRP10-deficient and C3H/HeJ mice results in defective dendritic cell migration. Proc. Natl. Acad. Sci. USA *112*, 3056–3061.

Krishnaswamy, J.K., Gowthaman, U., Zhang, B., Mattsson, J., Szeponik, L., Liu, D., Wu, R., White, T., Calabro, S., Xu, L., et al. (2017). Migratory CD11b+ conventional dendritic cells induce T follicular helper cell-dependent antibody responses. Sci. Immunol. *2*, eaam9169.

Kunisaki, Y., Nishikimi, A., Tanaka, Y., Takii, R., Noda, M., Inayoshi, A., Watanabe, K., Sanematsu, F., Sasazuki, T., Sasaki, T., and Fukui, Y. (2006). DOCK2 is a Rac activator that regulates motility and polarity during neutrophil chemotaxis. J. Cell Biol. *174*, 647–652.

Lambe, T., Crawford, G., Johnson, A.L., Crockford, T.L., Bouriez-Jones, T., Smyth, A.M., Pham, T.H., Zhang, Q., Freeman, A.F., Cyster, J.G., et al. (2011). DOCK8 is essential for T-cell survival and the maintenance of $CD8^+$ T-cell memory. Eur. J. Immunol. *41*, 3423–3435.

Mabbott, N.A., Donaldson, D.S., Ohno, H., Williams, I.R., and Mahajan, A. (2013). Microfold (M) cells: important immunosurveillance posts in the intestinal epithelium. Mucosal Immunol. *6*, 666–677.

Mizesko, M.C., Banerjee, P.P., Monaco-Shawver, L., Mace, E.M., Bernal, W.E., Sawalle-Belohradsky, J., Belohradsky, B.H., Heinz, V., Freeman, A.F., Sullivan, K.E., et al. (2013). Defective actin accumulation impairs human natural killer cell function in patients with dedicator of cytokinesis 8 deficiency. J. Allergy Clin. Immunol. *131*, 840–848.

Nagashima, K., Sawa, S., Nitta, T., Tsutsumi, M., Okamura, T., Penninger, J.M., Nakashima, T., and Takayanagi, H. (2017). Identification of subepithelial mesenchymal cells that induce IgA and diversify gut microbiota. Nat. Immunol. *18*, 675–682.

Nishikimi, A., Fukuhara, H., Su, W., Hongu, T., Takasuga, S., Mihara, H., Cao, Q., Sanematsu, F., Kanai, M., Hasegawa, H., et al. (2009). Sequential regulation of DOCK2 dynamics by two phospholipids during neutrophil chemotaxis. Science *324*, 384–387.

Novitskaya, V., Grigorian, M., Kriajevska, M., Tarabykina, S., Bronstein, I., Berezin, V., Bock, E., and Lukanidin, E. (2000). Oligomeric forms of the metastasis-related Mts1 (S100A4) protein stimulate neuronal differentiation in cultures of rat hippocampal neurons. J. Biol. Chem. *275*, 41278–41286.

Ohtani, O., Kikuta, A., Ohtsuka, A., and Murakami, T. (1991). Organization of the reticular network of rabbit Peyer's patches. Anat. Rec. *229*, 251–258.

Österreicher, C.H., Penz-Österreicher, M., Grivennikov, S.I., Guma, M., Koltsova, E.K., Datz, C., Sasik, R., Hardiman, G., Karin, M., and Brenner, D.A. (2011). Fibroblast-specific protein 1 identifies an inflammatory subpopulation of macrophages in the liver. Proc. Natl. Acad. Sci. USA *108*, 308–313.

Pabst, O. (2012). New concepts in the generation and functions of IgA. Nat. Rev. Immunol. *12*, 821–832.

Pankratova, S., Klingelhöfer, J., Dmytriyeva, O., Owczarek, S., Renziehausen, A., Syed, N., Porter, A.E., Dexter, D.T., and Kiryushko, D. (2018). The S100A4 protein signals through the ErbB4 receptor to promote neuronal survival. Theranostics *8*, 3977–3990.

Randall, K.L., Lambe, T., Johnson, A.L., Treanor, B., Kucharska, E., Domaschenz, H., Whittle, B., Tze, L.E., Enders, A., Crockford, T.L., et al. (2009). Dock8 mutations cripple B cell immunological synapses, germinal centers and long-lived antibody production. Nat. Immunol. *10*, 1283–1291.

Randall, K.L., Chan, S.S., Ma, C.S., Fung, I., Mei, Y., Yabas, M., Tan, A., Arkwright, P.D., Al Suwairi, W., Lugo Reyes, S.O., et al. (2011). DOCK8 deficiency impairs CD8 T cell survival and function in humans and mice. J. Exp. Med. *208*, 2305–2320.

Rickert, R.C., Rajewsky, K., and Roes, J. (1995). Impairment of T-cell-dependent B-cell responses and B-1 cell development in CD19-deficient mice. Nature *376*, 352–355.

Rios, D., Wood, M.B., Li, J., Chassaing, B., Gewirtz, A.T., and Williams, I.R. (2016). Antigen sampling by intestinal M cells is the principal pathway initiating mucosal IgA production to commensal enteric bacteria. Mucosal Immunol. *9*, 907–916.

Ruusala, A., and Aspenström, P. (2004). Isolation and characterisation of DOCK8, a member of the DOCK180-related regulators of cell morphology. FEBS Lett. *572*, 159–166.

Sanal, O., Jing, H., Ozgur, T., Ayvaz, D., Strauss-Albee, D.M., Ersoy-Evans, S., Tezcan, I., Turkkani, G., Matthews, H.F., Haliloglu, G., et al. (2012). Additional diverse findings expand the clinical presentation of DOCK8 deficiency. J. Clin. Immunol. *32*, 698–708.

Sato, S., Kaneto, S., Shibata, N., Takahashi, Y., Okura, H., Yuki, Y., Kunisawa, J., and Kiyono, H. (2013). Transcription factor Spi-B-dependent and -independent pathways for the development of Peyer's patch M cells. Mucosal Immunol. *6*, 838–846.

Sawa, S., Cherrier, M., Lochner, M., Satoh-Takayama, N., Fehling, H.J., Langa, F., Di Santo, J.P., and Eberl, G. (2010). Lineage relationship analysis of RORgammat+ innate lymphoid cells. Science *330*, 665–669.

Schneider, M., Hansen, J.L., and Sheikh, S.P. (2008). S100A4: a common mediator of epithelial-mesenchymal transition, fibrosis and regeneration in diseases? J. Mol. Med. (Berl.) *86*, 507–522.

Shiraishi, A., Uruno, T., Sanematsu, F., Ushijima, M., Sakata, D., Hara, T., and Fukui, Y. (2017). DOCK8 protein regulates macrophage migration through Cdc42 protein activation and LRAP35a protein interaction. J. Biol. Chem. *292*, 2191–2202.

Singh, A.K., Eken, A., Fry, M., Bettelli, E., and Oukka, M. (2014). DOCK8 regulates protective immunity by controlling the function and survival of RORγt+ ILCs. Nat. Commun. *5*, 4603.

Sun, J.B., Holmgren, J., Larena, M., Terrinoni, M., Fang, Y., Bresnick, A.R., and Xiang, Z. (2017). Deficiency in calcium-binding protein S100A4 impairs the adjuvant action of cholera toxin. Front. Immunol. *8*, 1119.

Suzuki, K., Meek, B., Doi, Y., Muramatsu, M., Chiba, T., Honjo, T., and Fagarasan, S. (2004). Aberrant expansion of segmented filamentous bacteria in IgA-deficient gut. Proc. Natl. Acad. Sci. USA *101*, 1981–1986.

Terahara, K., Yoshida, M., Igarashi, O., Nochi, T., Pontes, G.S., Hase, K., Ohno, H., Kurokawa, S., Mejima, M., Takayama, N., et al. (2008). Comprehensive gene expression profiling of Peyer's patch M cells, villous M-like cells, and intestinal epithelial cells. J. Immunol. *180*, 7840–7846.

Ushijima, M., Uruno, T., Nishikimi, A., Sanematsu, F., Kamikaseda, Y., Kunimura, K., Sakata, D., Okada, T., and Fukui, Y. (2018). The Rac activator DOCK2 mediates plasma cell differentiation and IgG antibody production. Front. Immunol. *9*, 243.

Yamamura, K., Uruno, T., Shiraishi, A., Tanaka, Y., Ushijima, M., Nakahara, T., Watanabe, M., Kido-Nakahara, M., Tsuge, I., Furue, M., and Fukui, Y. (2017). The transcription factor EPAS1 links DOCK8 deficiency to atopic skin inflammation via IL-31 induction. Nat. Commun. *8*, 13946.

Zhang, Q., Davis, J.C., Lamborn, I.T., Freeman, A.F., Jing, H., Favreau, A.J., Matthews, H.F., Davis, J., Turner, M.L., Uzel, G., et al. (2009). Combined immunodeficiency associated with DOCK8 mutations. N. Engl. J. Med. *361*, 2046–2055.

Zhang, Q., Davis, J.C., Dove, C.G., and Su, H.C. (2010). Genetic, clinical, and laboratory markers for DOCK8 immunodeficiency syndrome. Dis. Markers *29*, 131–139.

Zhang, Q., Dove, C.G., Hor, J.L., Murdock, H.M., Strauss-Albee, D.M., Garcia, J.A., Mandl, J.N., Grodick, R.A., Jing, H., Chandler-Brown, D.B., et al. (2014). DOCK8 regulates lymphocyte shape integrity for skin antiviral immunity. J. Exp. Med. *211*, 2549–2566.

Zhang, W., Ohno, S., Steer, B., Klee, S., Staab-Weijnitz, C.A., Wagner, D., Lehmann, M., Stoeger, T., Königshoff, M., and Adler, H. (2018). S100a4 is secreted by alternatively activated alveolar macrophages and promotes activation of lung fibroblasts in pulmonary fibrosis. Front. Immunol. *9*, 1216.

STAR★METHODS

KEY RESOURCES TABLE

REAGENT or RESOURCE	SOURCE	IDENTIFIER
Antibodies		
Goat anti-mouse IgA-AP	Southern Biotech	Cat#1040-04; RRID: AB_2794372
APC-conjugated anti-mouse IgD (11-26c.2a)	BioLegend	Cat#405714; RRID: AB_10643423
PE-conjugated anti-mouse Podoplanin (8.1.1)	BioLegend	Cat#127408; RRID: AB_2161928
Alexa Fluor 488-conjugated anti-mouse MAdCAM-1 (MECA-367)	BioLegend	Cat#120708; RRID: AB_493398
Goat anti-mouse TRANCE / RANKL / TNFSF11 biotinylated	R&D systems	Cat#BAF462; RRID: AB_2287613
Alexa Fluor 647-conjugated streptavidin	Thermo Fisher Scientific	Cat#S21374; RRID: AB_2336066
APC-conjugated anti-CD11c (N418)	BioLegend	Cat#117310; RRID: AB_313779
PE-conjugated anti-CD11c (N418)	BioLegend	Cat#117308; RRID: AB_313777
PE-conjugated anti-CD90.2 (53-2.1)	BD Biosciences	Cat#553006; RRID: AB_394545
FITC-conjugated anti-mouse CD4 (RM4-5)	BD Biosciences	Cat#553047; RRID: AB_394583
PE-conjugated anti-mouse GP2 (2F11-C3)	MBL	Cat#D278-5; RRID: AB_11160946
Rabbit anti-mouse AnnexinV	Abcam	Cat#ab14196; RRID: AB_300979
Alexa Fluor 488-conjugated donkey anti-rabbit IgG (H+L) Ab	Thermo Fisher Scientific	Cat# A21206; RRID: AB_141708
Rabbit anti-mouse E-cadherin (24E10)	CST	Cat#3195; RRID: AB_2291471
Rabbit anti-mouse Collagen Type I biotinylated	Rockland	Cat#600-406-103; RRID: AB_217579
Rabbit anti-mouse DOCK8 N terminus (MTHLNSLDAELAQELGDLT)	This paper	N/A
Rabbit anti-human/mouse DOCK8 C terminus (RDSFHRSSFRKCETQLSQGS)	Yamamura et al., 2017	N/A
Goat anti-mouse βactin Ab (I-19)	Santa Cruz	Cat#sc-1616; RRID: AB_630836
Rabbit anti-mouse S100A4	Abcam	Cat#ab41532; RRID: AB_945346
Rat anti-mouse CD16/32 (Fcγ III/II receptor; 2.4G2) purified	TONBO biosciences	Cat#70-0161; RRID: AB_2621487
PE-conjugated anti-mouse BST-2 (927)	BioLegend	Cat#127010; RRID: AB_1953285
PerCP-5.5cyanine-conjugated anti-mouse Sca-1 (D7)	eBiosciences	Cat#45-5981-82; RRID: AB_914372
PE-conjugated anti-human/mouse B220 (RA3-6B2)	TONBO biosciences	Cat#50-0452; RRID: AB_2621764
PE-conjugated anti-mouse CD3ε (17A2)	BioLegend	Cat#100206; RRID: AB_312663
PE-conjugated anti-mouse CD8α (53-6.7)	TONBO biosciences	Cat#50-0081; RRID: AB_2621741
PE-conjugated anti-mouse CD11b (M1/70)	BD Biosciences	Cat#557397; RRID: AB_396680
PE-conjugated anti-mouse Ly6G/Ly6C (RB6-8C5)	BD Biosciences	Cat#553128; RRID: AB_394644
PE-conjugated anti-mouse NK1.1 (PK136)	BD Biosciences	Cat#557391; RRID: AB_396674
PE-conjugated anti-mouse FcεR1 (MAR-1)	TONBO biosciences	Cat#50-5898; RRID: AB_2621801
Biotin anti-mouse CD117 (c-Kit) (2B8)	BD Biosciences	Cat#553353; RRID: AB_394804
APC-conjugated Streptavidin	BD Biosciences	Cat#554067; RRID: AB_10050396
Sheep anti-human/mouse S100A4 antibody	R&D systems	Cat#AF4138; RRID: AB_1964705
EGF Receptor (D1D4J) XP rabbit monoclonal antibody (Neutralizing)	CST	Cat#54359S; RRID: AB_2799458
Bacterial and Virus Strains		
Salmonella Choleraesuis, strain RF-1	Kawahara et al., 1988	N/A

(*Continued on next page*)

Continued

REAGENT or RESOURCE	SOURCE	IDENTIFIER
Chemicals, Peptides, and Recombinant Proteins		
Cholera toxin (Azide-free) from *Vibrio cholerae*	List Biological Laboratories	Cat#100B
Albumin from chicken egg white	Sigma-Aldrich	Cat#A5503
Casein sodium	Wako	Cat#143-02845
Polyoxyethylene(20) sorbitan monolaurate (Tween-20)	Wako	Cat#166-21115
D-PBS (-)	Wako	Cat#045-29795
Sucrose	Wako	Cat#196-00015
HBSS (-)	Thermo Fisher Scientific	Cat#14175-095
Paraformaldehyde	Sigma-Aldrich	Cat#P6148; CAS: 30525-89-4
PLP (periodate–lysine-paraformaldehyde) solution set	Wako	Cat#290-63201
Fluoresbrite Plain YG 0.2Micron Microspheres	Polysciences	Cat#17151-10
O.C.T. Compound	Sakura Finetech	Cat#4583-B
Bovine serum albumin (BSA)	Sigma-Aldrich	Cat#A4503; CAS: 9048-46-8
DAPI solution	Dojindo Laboratories	Cat#340-07971
Ethanol (99.5)	Wako	Cat#057-00456; CAS: 64-17-5
Gentamicin Sulfate	Wako	Cat#079-02973; CAS: 1405-41-0
Collagenase D	Roche	Cat#11088866001
Dispase II	Roche	Cat#04942078001
DNase I	Roche	Cat#11284932001
RPMI-1640	Wako	Cat#189-02025
Fatal Bovine Serum	Thermo Fisher Scientific	Cat#10270-106
2-Mercaptoethanol	Nacalai Tesque	Cat#21418-42; CAS: 60-24-2
L-Glutamine (200 mM)	Thermo Fisher Scientific	Cat#25030-081
Sodium Pyruvate (100 mM)	Thermo Fisher Scientific	Cat#11360-070
MEM non-essential amino acids (100x)	Thermo Fisher Scientific	Cat#11140-050
cOmplete, protease inhibitor cocktail	Roche	Cat#13539320
Matrigel Basement Membrane Matrix	Corning	Cat#354234
Advanced DMEM/F12	Thermo Fisher Scientific	Cat#12634-010
GlutaMAX	Thermo Fisher Scientific	Cat#35050061
N-2 supplement	Thermo Fisher Scientific	Cat#17502001
B-27 supplement minus vitamin A	Thermo Fisher Scientific	Cat#12587010
N-acetylcysteine	Sigma-Aldrich	Cat#A9165
HEPES buffer solution	Sigma-Aldrich	Cat#83264; CAS: 7365-45-9
Pen Strep (Penicillin-Streptomycin)	Thermo Fisher Scientific	Cat#15140-122
Recombinant murine Noggin	PeproTech	Cat#250-38
Recombinant murine RANKL	PeproTech	Cat#315-11
Recombinant mouse R-spondin1 protein	R&D systems	Cat#3474-RS-050
Recombinant mouse S100A4 protein	R&D systems	Cat#4138-S4
Recombinant murine EGF	PeproTech	Cat#315-09
Recombinant mouse CX3CL1 protein	R&D systems	Cat#472-FF-025
Recombinant mouse CCL5 protein	R&D systems	Cat#478-MR-025
Recombinant murine M-CSF	PeproTech	Cat#315-02
Tyrphostin AG1478	Sigma-Aldrich	Cat#T4182; CAS: 175178-82-2
Tyrphostin AG879	Sigma-Aldrich	Cat#T2067; CAS: 148741-30-4
SU5402	Sigma-Aldrich	Cat#SML0443; CAS: 215543-92-3
KRN633	Sigma-Aldrich	Cat#SML0957; CAS: 286370-15-8
RAGE antagonist, FPS-ZM1	Merck	Cat#553030
Dimethyl Sulfoxide (DMSO)	Wako	Cat#043-29355

(*Continued on next page*)

Continued

REAGENT or RESOURCE	SOURCE	IDENTIFIER
PhosSTOP, phosphatase inhibitor	Sigma	Cat#4906845001
Cell Recovery Solution	Corning	Cat#354253
Collagen Type I, Rat tail	Corning	Cat#354236
DNase I, Amplification Grade	Thermo Fisher Scientific	Cat#18068015
Oligo(dT)$_{12-18}$ primer	Thermo Fisher Scientific	Cat#18418012
SuperScript III Reverse Transcriptase	Thermo Fisher Scientific	Cat#18080044
Critical Commercial Assays		
Cytofix/Cytoperm Kit	BD Biosciences	Cat#554714
DC Protein Assay Reagents	BioRad	Cat#5000116JA
ECL Western Blotting Detection Reagent	GE Healthcare	Cat#RPN2106
μ-Slide Chemotaxis^{3D}	ibidi	Cat#ib80326
Trans AM NFκB family assay kit	Active Motif	Cat#43296
ISOGEN	Nippon Gene	Cat#311-02501
PowerSYBR Green PCR Master Mix	Thermo Fisher Scientific	Cat#4367659
Low Input Quick Amp Labeling Kit	Agilent Technologies	Cat#5190-2306
SurePrint G3 Mouse Gene Expression Microarray 8x60K Ver 2.0	Agilent Technologies	Cat#G4852B
ISOSPIN Fecal DNA	Nippon Gene	Cat#315-08621
MiSeq Reagent Kit v3	Illumina	Cat#MS-102-3003
Deposited Data		
Microarray data (S100A4-GFP positive and negative cells)	This paper	GEO: GSE127686
RNA-seq data (Follicle-associated epithelia of *Tnfrsf11a* $^{fl/\Delta}$ mice)	Nagashima et al., 2017	GEO: GSE93319
Experimental Models: Organisms/Strains		
Mouse: C57BL/6JJcl	CLEA Japan	RRID: MGI: 5658466
Mouse: B6.Cg-Tg(S100a4-EGFP)M1Egn/YunkJ (S100A4-EGFP)	Jackson Laboratory	RRID: IMSR_JAX: 012893
Mouse: B6.Cg-Tg(Itgax-cre)1-1Reiz/J (*Itgax*-Cre / CD11c-Cre)	Jackson Laboratory	RRID: IMSR_JAX: 008068
Mouse: B6N.Cg-Tg(Vil1-cre/ERT2)23Syr/J (*Villin*-Cre)	Sylvie Robine	RRID: IMSR_JAX: 020282
Mouse: *Twist2*$^{tm1.1(cre)Dor}$ (*Twist2*-Cre)	David Ornitz	RRID: IMSR_JAX: 008712
Mouse: B6.129P2-Lyz2$^{tm1(cre)Ifo}$ /J (*Lyz2*-Cre)	Irmgard Foerster	RRID: IMSR_JAX: 004781
Mouse: BALB/c-Tg(S100a4-cre)1Egn/YunkJ (*S100a4*-Cre)	Eric G. Neilson	RRID: IMSR_JAX: 012641
Mouse: Lyz2$^{tm1.1Graf}$ (LysM-EGFP)	Thomas Graf	RRID: MGI: 2654932
Mouse: B6.FVB-Tg(Rorc-cre)^{1Litt} /J (*Rorc*-Cre)	Gerard Eberl	RRID: IMSR_JAX: 022791
Mouse: Tg(Rorc-EGFP)1Ebe (RORγt-EGFP)	Gerard Eberl	RRID: MGI: 3829387
Mouse: B6.129P2(C)-*Cd19*$^{tm1(cre)Cgn}$/J (*Cd19*-Cre)	Klaus Rajewsky	RRID: IMSR_JAX: 006785
Mouse: Dock2^{tm1Ysfk} (DOCK2-GFP)	Kunisaki et al., 2006	RRID: MGI: 3772947
Mouse: *Dock8* ^{tm1Ysfk} (*Dock8*$^{-/-}$)	Harada et al., 2012	RRID: MGI: 5437279
Mouse: *Dock8*^{loxlox}	This paper	N/A
Mouse: *S100a4*$^{-/-}$	This paper	N/A
Oligonucleotides		
Mouse primers for conventional RT-PCR and real-time PCR, see Table S1	This paper	N/A
Recombinant DNA		
Plasmid: pX330-U6-Chimeric_BB-CBh-hSpCas9	Cong et al., 2013	RRID: Addgene_42230

(*Continued on next page*)

Continued

REAGENT or RESOURCE	SOURCE	IDENTIFIER
Software and Algorithms		
ImageJ	National Institute of Health (NIH)	RRID: SCR_003070
FV31S-DT, cellSens Dimension	Olympus	RRID: SCR_016238
MetaMorph	Molecular Devices	RRID: SCR_002368
Bio-Rad CFX Manager ver. 3.1	BioRad	RRID: SCR_017251
BD FACSuite	BD Biosciences	https://www.bdbiosciences.com/
Feature Extraction Software version 9.5.1.1	Agilent Technologies	RRID: SCR_014963
Flora Genesis software	Repertoire Genesis	https://www.repertoire.co.jp/
Prism7.0	Graphpad	RRID: SCR_002798

LEAD CONTACT AND MATERIALS AVAILABILITY

Further information and requests for resources and reagents should be directed to and will be fulfilled by the Lead Contact, Yoshinori Fukui (fukui@bioreg.kyushu-u.ac.jp). All unique reagents and mouse lines generated in this study are available from the Lead Contact with a completed Materials Transfer Agreement.

EXPERIMENTAL MODEL AND SUBJECT DETAILS

Animals

Dock8$^{-/-}$ mice have been described previously (Harada et al., 2012; Yamamura et al., 2017). Mice heterozygous for the mutant allele (*Dock8*$^{+/-}$) were backcrossed onto a C57BL/6 background for more than nine generations, and *Dock8*$^{+/-}$ littermate mice were used as controls. *Dock8*$^{lox/lox}$ mice have been developed by homologous recombination in embryonic stem (ES) cells (Figure S2A). Briefly, the targeting vector was constructed using the pNT1.1 vector, which contains 4.9-kb 5′- and 4.2-kb 3′-homologous arms, a 0.6-kb fragment of the mouse *Dock8* gene encoding exon 3 flanked by two *loxP* sites, the PGK-neo cassette (*Neo*) flanked by two flippase recognition target (FRT) sites, and HSV-thymidine kinase cassette (*TK*) at the distal end of the 5′-arm. The targeting vector was linearized by *Not* I, and electroporated into ES cells from C57BL/6 mice. Correctly targeted ES cells were injected into BALB/c blastocysts, and chimeric male founders were crossed with C57BL/6 female mice. The germline transmission of the recombinant allele was confirmed by PCR and Southern blot analysis. The PGK-neo cassette was excised by crossing with the *CAG-FLPe* transgenic mice. The *FLP* gene was subsequently removed by breeding. *Cre*-mediated excision of exon 3 results in appearance of a premature stop codon in exon 4. Genotyping of the wild-type, conditional, and deleted alleles was carried out by PCR with the following primers: F1, 5′-CCTGCATGTGGCCTTCACACC-3′; R6, 5′-TGCTGCTCTGTAGCCCTTCC-3′; F7, 5′-GCTGCGTTTGCCTGAGTTTCTGGAG-3′ (Figure S2). C57BL/6 mice were obtained from CLEA Japan. S100A4-GFP mice (Iwano et al., 2002) and *CD11c (Itgax)-Cre* Tg (Caton et al., 2007) mice were purchased from the Jackson Laboratory. *Vil1-CreER*^{T2} mice were used after intraperitoneal injection of tamoxifen (1 mg/mouse) for 5 consecutive days (el Marjou et al., 2004). *Twist2-Cre* knock-in mice (Geske et al., 2008), *Lyz2-Cre* knock-in mice (Clausen et al., 1999), *S100a4-Cre* Tg mice (Bhowmick et al., 2004), lysozyme-M-GFP mice (Faust et al., 2000), *Cd19-Cre* knock-in mice (Rickert et al., 1995), BAC-transgenic *Rorc-Cre* Tg mice (Sawa et al., 2010), RORγt-GFP Tg mice (Sawa et al., 2010) and DOCK2-GFP knock-in mice (Kunisaki et al., 2006; Nishikimi et al., 2009) have been described elsewhere. *S100a4*$^{-/-}$ mice have been generated by CRISPR/Cas9 system (Figure S6). A targeting site within the exon 2 of mouse *S100a4* was selected using the CHOPCHOP web design tool (http://chopchop.cbu.uib.no/). Two complementary oligonucleotides (5′- CACCGCTCAAGG AGCTACTGACCA −3′ and 5′- AAACTGGTCAGTAGCTCCTTGAGC −3′) containing the guide sequence and *Bbs I* ligation adaptors were synthesized, annealed, and ligated into the *Bbs I*–digested px330 vector for coexpression of single guide RNA (sgRNA) and Cas9 protein. The pX330 vector (5 ng/mL in PBS) was injected into the pronuclei of *in vitro* fertilized eggs of C57BL/6 mice in M2 medium (Sigma-Aldrich). The injected zygotes were cultured in CZB medium at 37°C, 5% CO_2 until 2-cell stage embryos develop. Then, 24 to 36 embryos were transferred into the oviducts of pseudopregnant ICR female mice. The offspring mice carrying desired mutation (Δ7) were crossed with C57BL/6 mice. In all experiments, the littermate mice of both sexes were used at 6–10 weeks old. Mice were selected randomly and assigned to experimental groups according to genotype. The investigators who performed the experiments were not blinded to mouse genotypes. Mice were maintained under specific-pathogen-free conditions in the animal facility of Kyushu University. The protocol of animal experiments was performed in accordance with the guidelines of the committee of Ethics Animal Experiments of Kyushu University.

Bacterial Strains

Salmonella Choleraesuis strain RF-1 used in this study has been described previously (Kawahara et al., 1988). The bacteria were grown in tryptic soy broth at 37°C, harvested, then suspended in phosphate-buffered saline (PBS) containing 10% glycerol and

stored at –80°C in small aliquots until use. The concentration of bacteria was quantified by plate counting. Before use, the bacteria were washed three times with PBS and resuspended in PBS.

METHOD DETAILS

Oral Immunization and ELISA

Before immunization with CTX, mice were deprived of food for 2 h and then given 0.25 mL of a solution containing eight parts of Hanks balanced salt solution (HBSS) and two parts of 7.5% sodium bicarbonate by oral gavage to neutralize stomach acidity. After 30 min, mice were orally immunized with 30 μg CTX (List Biological Laboratories). Serum and fecal pellets were collected 14 days after immunization and were analyzed by ELISA as previously described (Ushijima et al., 2018). Briefly, 96-well polystyrene plates (Thermo 3855) were coated overnight at 4°C with CTX (0.5 μg/well; List Biological Laboratories) or OVA (0.5 μg/well; Sigma-Aldrich). After the wells were blocked with PBS containing 1% sodium casein (Wako) and 0.1% Tween-20 (Wako), serial dilutions of sera were added to the well. Alkaline phosphatase-conjugated IgA antibody (Southern Biotech) was used to detect bound antibody. The reactions were visualized with the substrate p-nitrophenyl phosphate (Sigma-Aldrich) and detected at 405 nm.

Uptake of Orally Administered Particles and Bacteria by M Cells

Fluorescent polystyrene latex nanoparticles (1×10^{11}) with 200-nm diameter (Fluoresbrite YG; Polysciences) were orally administered into mice. After 3 h, PPs were dissected, fixed in 3.7% paraformaldehyde (Sigma-Aldrich) in PBS for 2 h, and incubated overnight with 30% sucrose (Wako) in PBS at 4°C. Samples were then embedded in O.C.T. compound (Sakura Finetech) and frozen at –80°C. Cryostat sections (5 μm thick) were stained with the indicated antibodies and DAPI solution (Dojindo Laboratories; 1:5,000) for analyses using a laser scanning confocal microscope (FV3000; Olympus). The number of nanoparticles taken up into PPs was counted manually.

To measure uptake of bacteria, mice were orally infected with 1×10^{10} CFU of *S.* Choleraesuis strain RF-1. After 24 h, PPs were dissected and incubated for 30 min at 20°C with gentle shaking in sterile PBS containing 100 μg/ml gentamicin (Wako). After being washed thoroughly with PBS, pooled PP tissues were weighed and homogenized in sterile PBS. The tissue homogenates of PPs were serially diluted in sterile PBS and were plated on tryptic soy agar plates, and 24h later, the colonies of bacteria were counted to determine the CFU.

Whole Mount Immunostaining

PPs were excised and fixed with Cytofix/Cytoperm kit (BD Biosciences). The whole mount specimens were stained with PE-conjugated anti-GP2 antibody (MBL; 1:10) and DAPI solution (Dojindo Laboratories; 1:5,000). Images were obtained with a laser scanning confocal microscope (FV3000; Olympus). The number of $GP2^+$ mature M cells per field of FAE were analyzed using cellSens Dimension software (Olympus).

Immunohistochemistry

For analysis of tissue sections, PPs were dissected from the small intestine and fixed in 1% periodate–lysine-paraformaldehyde (PLP) (Wako) overnight at 4°C. Then, fixed tissues were incubated overnight with 30% sucrose in PBS at 4°C and embedded in O.C.T. compound (Sakura Finetech). After being frozen at –80°C, cryostat sections (5 μm thick) were blocked with 1% bovine serum albumin (BSA; Sigma-Aldrich) and anti-mouse CD16/32 (Fcγ III/II receptor; 2.4G2) (1:1,000) in PBS containing 0.1% Tween-20 (Wako) for 1 h at room temperature. Samples were then stained with the following antibodies: anti-mouse IgD (1:100), anti-mouse Podoplanin (1:100), anti-mouse MAdCAM-1 (1:100), biotinylated anti-mouse RANKL (1:100), anti-mouse CD11c (1:100), anti-mouse CD90.2 (1:100), anti-mouse CD4 (1:100), anti-mouse Gp2 (1:10), anti-mouse AnnexinV (1:200), anti-mouse E-cadherin (1:200), biotinylated anti-mouse Collagen Type I (1:100), Alexa Fluor 647-conjugated streptavidin (1:500) and/or Alexa Fluor 488-conjugated anti-rabbit IgG (1:500). Polyclonal antibody against DOCK8 was produced by immunizing rabbits with KLH-coupled synthetic peptide corresponding to the N-terminal sequence of mouse DOCK8 (MTHLNSLDAELAQELGDLT, residues 69-87) and was used for immunohistochemistry (0.09 mg/mL; 1:100). All images were obtained with a laser scanning confocal microscope (FV3000; Olympus).

Scanning Electron Microscopy

PPs were excised and fixed with 2.5% glutaraldehyde in 0.1 M cacodylate buffer (pH 7.4) for 16 h at 4°C. After being rinsed in phosphate buffer (pH 7.4), the tissues were post-fixed with 1% OsO4 solution on ice for 1 h and dehydrated in a graded series of ethanol (Wako). Then, tissues were substituted with *t*-butyl alcohol (Wako). After being freeze-dried, tissues were metal-coated, and examined by scanning electron microscopy (TM3000; Hitachi).

Isolation of Cells from Mouse Tissues

The isolation of cells from PPs was performed as previously described (Nagashima et al., 2017). Briefly, PPs were dissected, cut into pieces and incubated for 60 min at 37°C with fresh DMEM containing dispase II (Roche), collagenase D (Roche) and DNase I (Roche). Every 15 min, tissues were washed with warm DMEM and re-incubated with fresh medium containing dispase II, collagenase D and DNase I. The supernatant was collected at each step. Small intestinal epithelial cells were isolated as described previously

(Terahara et al., 2008). Briefly, small intestines were treated with 0.5 mM EDTA in PBS for 20 min at 37°C. Dissociated cells were filtered through 40-μm cell strainer (BD Biosciences) and centrifuged before assays.

BM-Derived Macrophage Culture

After being flushed from the femur and tibia from mice, BM cells were incubated in 10 mL of RPMI-1640 medium (Wako) containing 10% heat-inactivated fetal bovine serum (Thermo Fisher Scientific), 100 units/mL penicillin (Thermo Fisher Scientific), 100 μg/mL streptomycin (Thermo Fisher Scientific), 50 μM 2-mercaptoethanol (Nacalai Tesque), 2 mM L-glutamine (Thermo Fisher Scientific), 1 mM sodium pyruvate (Thermo Fisher Scientific), 1x MEM non-essential amino acids (Thermo Fisher Scientific) and recombinant M-CSF (Peprotech; 20 ng/mL). Cells were collected at day 7 and used for immunoblotting.

Immunoblotting

BM-derived macrophages and isolated intestinal epithelial cells were lysed on ice in 20 mM Tris-HCl buffer (pH 7.5) containing 1% Triton X-100, 150 mM NaCl, 1 mM EDTA, 1 mM EGTA, 2.5 mM sodium pyrophosphate, 1 mM β-glycerophosphate, 1 mM Na_3VO_4, and complete protease inhibitors (Roche). After centrifugation, the supernatants were mixed with an equal volume of 2 × sample buffer (125 mM Tris-HCl, 0.01% bromophenol blue, 4% SDS, 20% glycerol and 200 μM dithiothreitol). Samples were boiled for 5 min and analyzed by immunoblotting. Cell extracts were separated by SDS-PAGE and immunoblotted with the following antibodies: goat anti-β actin (1:1,000), rabbit anti-E-cadherin (1:1,000) or rabbit anti-S100A4 (1:250). Polyclonal antibody against DOCK8 was produced by immunizing rabbits with KLH-coupled synthetic peptide corresponding to the C-terminal sequence of human and mouse DOCK8 (RDSFHRSSFRKCETQLSQGS, residues 2081-2100) and used for immunoblotting (1.2 mg/mL; 1:1,000) (Yamamura et al., 2017; Shiraishi et al., 2017).

Intestinal Organoid Culture

Intestinal crypts were isolated and cultured as previously described (de Lau et al., 2012; Kanaya et al., 2018). Briefly, mouse intestine was cut longitudinally and washed with cold PBS. Villi were carefully scraped away and small pieces (5 mm) of intestine were incubated in 2 mM EDTA in PBS for 30 min on ice. These pieces were then vigorously suspended in cold PBS and the mixture was passed through 70-μm cell strainer (BD Biosciences). The crypt fraction was enriched through centrifugation (3 min at 200 x *g*). Then, the crypts were embedded in Matrigel (Corning) and seeded on 24-well plate. Crypts were cultured in Advanced DMEM/F12 (Thermo Fisher Scientific) containing glutamax (2 mM; Thermo Fisher Scientific), HEPES (10 mM; Sigma-Aldrich), penicillin-streptomycin (100 U/mL; Thermo Fisher Scientific), recombinant mouse R-spondin1 (1 μg/mL; R&D Systems), recombinant murine Noggin (100 ng/mL; PeproTech), N-2 supplement (Thermo Fisher Scientific), B-27 supplement minus Vitamin A (Thermo Fisher Scientific), and *N*-acetylcysteine (1 mM; Sigma-Aldrich). S100A4-positive or -negative cells ($1x10^5$ cells/well) were seeded on the outside of the matrigel at day 0 in the presence or absence of anti-S100A4 antibody (20 μg/mL; R&D Systems). Recombinant murine EGF (50 ng/mL; PeproTech) or recombinant murine S100A4 protein (50 ng/mL; R&D Systems) was added to the culture on day 0. Recombinant murine RANKL (100 ng/mL; PeproTech) was added to the culture on day 5. In some experiments, the following tyrosine kinase inhibitors were added to the culture at day 5; AG1478 for ErbB1 (300 nM; Sigma-Aldrich), AG879 for Erb2 and TrkA (5 μM; Sigma-Aldrich), FPS-ZM1 for RAGE (10 μM; Merck), SU5402 for FGFR1, VEGFR2, and PDGFR (10 μM; Sigma-Aldrich), KRN633 for VEGFR1 and VEGFR3 (1 μM; Sigma-Aldrich). All compounds were dissolved in 100% dimethylsulfoxide (DMSO) and used at the DMSO concentration of 0.2%–0.01%. Anti-EGFR neutralizing antibody (10 μg/mL; CST) was added to the culture on day 5. Media were changed every 2 days and organoids were collected on day 10 for assays.

Flow Cytometry and Cell Sorting

Before staining with antibodies, cells were incubated for 10 min on ice with anti-mouse CD16/32 (Fcγ III/II receptor; 2.4G2) (1:1,000) to block Fc receptors. Cells were then stained with the following antibodies: anti-mouse BST2 (1:100), anti-mouse CD11c (1:100), anti-mouse Sca-1 (1:100), anti-mouse B220 (1:100), anti-mouse CD3ε (1:100), anti-mouse CD8α (1:100), anti-mouse CD11b (1:100), anti-mouse Ly6G/Ly6C (1:100), anti-mouse NK1.1 (1:100), anti-mouse FcεR1 (1:100), anti-mouse c-Kit (1:100) and/or APC-conjugated streptavidin (1:500). Flow cytometric analyses or sorting was performed with BD FACSVerse or BD FACSAria II (BD Biosciences), respectively. The sorted cells were of at least 95% purity. Data analysis was performed using BD FACSuite software (BD Biosciences).

3D Chemotaxis Assay

3D chemotaxis assays using collagen gel were performed with μ-Slide Chemotaxis^{3D} (ibidi), as described previously (Harada et al., 2012; Shiraishi et al., 2017). Briefly, sorted lysozyme-M-GFP$^+$ cells were mixed with 1.65 mg/mL of collagen type I (Corning) in RPMI medium (Wako) supplemented with 4% FCS and cast in the chamber before assays. After polymerization of the lattice, images of cells migrating toward CX3CL1 (400 ng/mL; R&D Systems) or CCL5 (100 ng/mL; R&D Systems) were taken in a heated chamber every 2 min using an IX-81 inverted microscope (Olympus) equipped with a cooled charge-coupled device camera (CoolSNAP HQ, Roper Scientific), an IX2-ZDC laser-based autofocusing system (Olympus), and an MD-XY60100T-Meta automatically programmable XY stage (Sigma KOKI). Images were taken by the MetaMorph software (Molecular Devices) and velocities were calculated with the manual tracking feature in the ImageJ software (National Institutes of Health).

ELISA for Measuring NFκB Activation

On day5, intestinal organoids were stimulated with recombinant S100A4 proteins (50 ng/mL; R&D Systems) and/or recombinant murine RANKL (100 ng/mL; PeproTech) for 12 h. Then, to dissolve Matrigel, intestinal organoids were incubated with Cell Recovery Solution (Corning) containing PhosSTOP phosphatase inhibitor (Roche) for 30 min on ice. Nuclear extracts of organoids were prepared using NE-PER Nuclear and Cytoplasmic Extraction Reagents (Thermo Fisher Scientific). Protein concentration of nuclear extracts was determined using DC Protein Assay Reagents (BioRad) and equal amounts of nuclear extracts (10 μg) were used in Trans AM NFκB family assay kit (Active Motif) according to the manufacturer's instructions. Briefly, each well contained the immobilized NF-κB consensus sequence of DNA (5′-GGGACTTTCC-3′) to which active NF-κB binds. The primary antibody (anti-p52 or anti-RelB) used in this assay only reacts to the epitope on the active p52 or RelB that is bound to its target DNA. Then, an HRP-conjugated secondary antibody was used to provide a sensitive colorimetric readout that is spectrophotometrically quantified.

Reverse Transcription-PCR

To dissolve Matrigel, intestinal organoids were incubated with Cell Recovery Solution (Corning) for 30 min on ice prior to RNA extraction. Total RNA was extracted from the sorted cells, intestinal organoids and isolated PPs with ISOGEN (Nippon Gene). After treatment with RNase-free DNase I (Thermo Fisher Scientific), RNA samples were reverse-transcribed with Oligo(dT)$_{12\text{-}18}$ primers (Thermo Fisher Scientific) and SuperScript III reverse transcriptase (Thermo Fisher Scientific) for amplification by PCR. Real-time PCR was performed on the CFX Connect Real-Time PCR Detection System (BioRad) using the SYBR Green PCR Master Mix (Thermo Fisher Scientific) according to the manufacturer's instructions. The expressions of target genes were normalized with *Hprt* expression. Melting curve analysis was performed to ensure the specificity of the amplification products. Sequence-detection software (Bio-Rad CFX Manager ver. 3.1) supplied with the instrument was used for analyses. The primers used for conventional reverse transcription-PCR and real-time PCR are listed in Table S1.

Microarray Analysis

Total RNA was isolated using ISOGEN (Nippon Gene), and cRNA was amplified and labeled using a Low Input Quick Amp Labeling Kit (Agilent Technologies). The cRNA was then hybridized to a 60 K 60-mer oligomicroarray (SurePrint G3 Mouse Gene Expression Microarray 8x60K Ver 2.0; Agilent Technologies). The hybridized microarray slides were scanned using an Agilent scanner. The relative hybridization intensities and background hybridization values were calculated using Feature Extraction Software version 9.5.1.1 (Agilent Technologies). Raw signal intensities and flags for each probe were calculated from the hybridization intensities and spot information, according to the procedures recommended by Agilent Technologies. Microarray data analysis was supported by Cell Innovator.

16S rRNA Gene Sequencing

The microbial DNA was extracted from mouse fecal samples using the ISOSPIN Fecal DNA (Nippon Gene). The V3-V4 region of 16S rRNA genes was amplified and sequenced by MiSeq Deep sequencer and MiSeq Reagent Kit v3 (Illumina) following manufacturer's instruction. The sequence data were preprocessed and analyzed using the Flora Genesis software (Repertoire Genesis). In brief, the R1 and R2 read pairs were joined and chimera sequences were removed. The operational taxonomic unit (OTU) picking was performed by the open-reference method using the 97% ID prefiltered Greengenes database and the uclust. The representative sequences of each OTU were chosen and taxonomy assignment was performed by RDP classifier using its threshold score 0.5 or more. The OTUs were grouped if their annotation was the same regardless of its RDP score. The 16S rRNA gene sequencing and data analysis were supported by Repertoire Genesis.

QUANTIFICATION AND STATISTICAL ANALYSIS

Statistical analyses were performed using Prism 7.0 (GraphPad Software). The data were initially tested with a Kolmogorov-Smirnov test for normal distribution. Parametric data were analyzed using a two-tailed unpaired Student's t test when two groups were compared. Nonparametric data were analyzed with a two-tailed Mann-Whitney test when two groups were compared. Statistical differences between more than two experimental groups were evaluated using analysis of variance (ANOVA) with Tukey's multiple-comparison test. *P*-values less than 0.05 were considered significant.

DATA AND CODE AVAILABILITY

The microarray data have been deposited in the Gene Expression Omnibus (GEO) repository under accession number GEO: GSE127686.

Cell Reports, Volume *29*

Supplemental Information

S100A4 Protein Is Essential for the Development of Mature Microfold Cells in Peyer's Patches

Kazufumi Kunimura, Daiji Sakata, Xin Tun, Takehito Uruno, Miho Ushijima, Tomoya Katakai, Akira Shiraishi, Ryosuke Aihara, Yasuhisa Kamikaseda, Keisuke Matsubara, Hirokazu Kanegane, Shinichiro Sawa, Gérard Eberl, Shouichi Ohga, Yasunobu Yoshikai, and Yoshinori Fukui

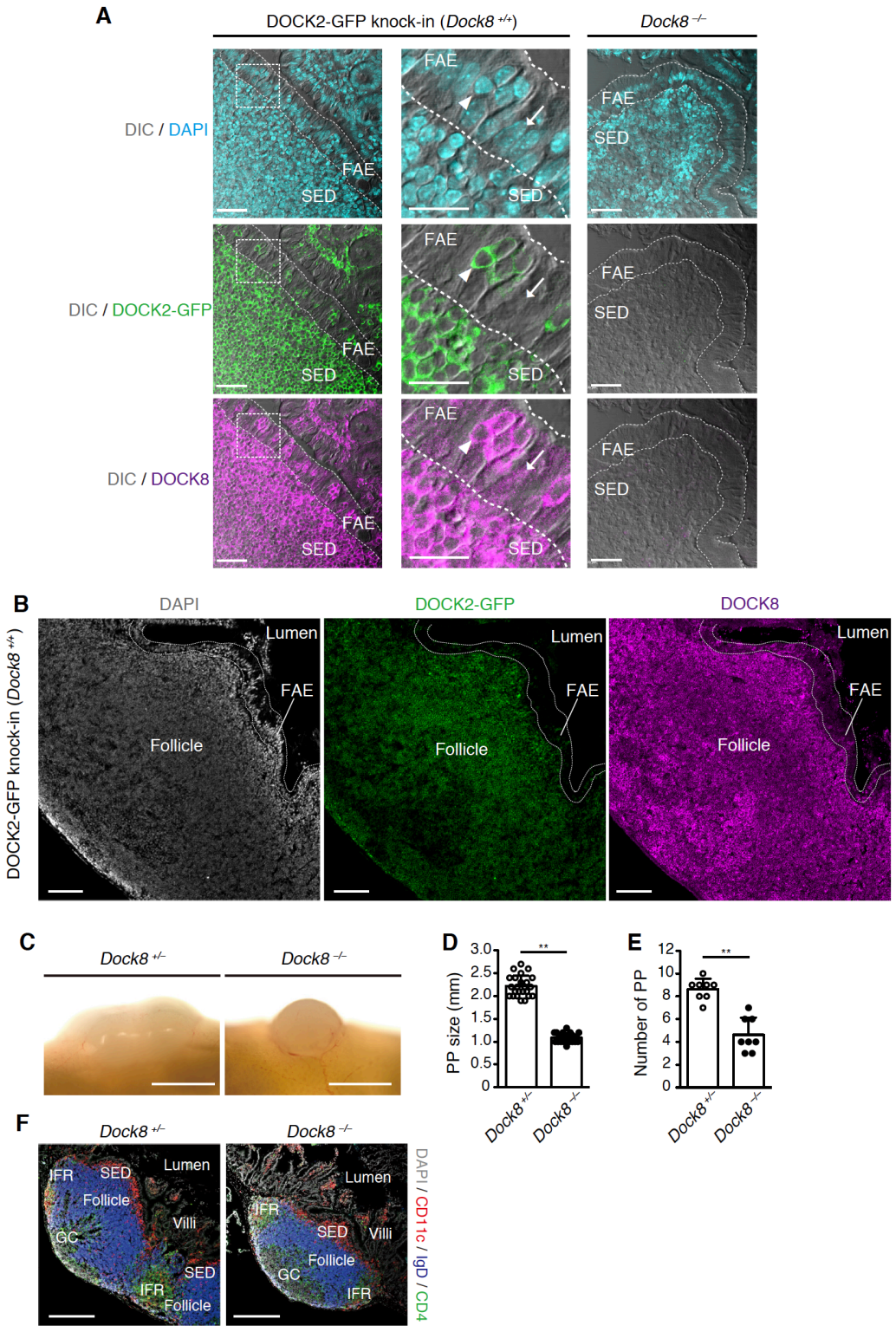

Figure S1. Overall comparison of PPs between *Dock8*$^{+/-}$ and *Dock8*$^{-/-}$ mice. Related to Figure 1.

(A and B) Immunohistochemical analyses for PPs from *Dock8*$^{-/-}$ mice and DOCK2-GFP knock-in mice (*Dock8*$^{+/+}$) that express endogenous DOCK2 as a fusion protein with GFP. Tissue sections were stained with anti-DOCK8 antibody and 4',6-Diamidino-2-phenylindole (DAPI). Arrows indicate follicle-associated epithelium (DOCK2-GFP^{-} DOCK8^{+}) and arrowheads indicate intraepithelial lymphocytes (DOCK2-GFP^{+} DOCK8^{+}). Higher magnification (middle column) of the area is outlined at left column. Scale bars, 40 μm (left and right column in A), 20 μm (middle column in A), and 100 μm (in B). The expression of DOCK2 is known to be largely restricted to hematopoietic cells. (C) A representative photograph of PPs in *Dock8*$^{+/-}$ and *Dock8*$^{-/-}$ mice. Scale bars, 1 mm.

(D) Comparison of the long diameter of each PP between *Dock8*$^{+/-}$ and *Dock8*$^{-/-}$ mice (n = 24 PPs from 4 different mice).

(E) Comparison of the number of PPs between *Dock8*$^{+/-}$ and *Dock8*$^{-/-}$ mice (n = 8).

(F) Immunohistochemical analyses for PPs from *Dock8*$^{+/-}$ and *Dock8*$^{-/-}$ mice. Tissue sections were stained for CD4, IgD, and CD11c with DAPI. Data are representative of three independent experiments. Scale bars, 300 μm. In (D and E), data are expressed as mean ± SD. $^{**}P < 0.01$ by two-tailed unpaired Student's *t*-test.

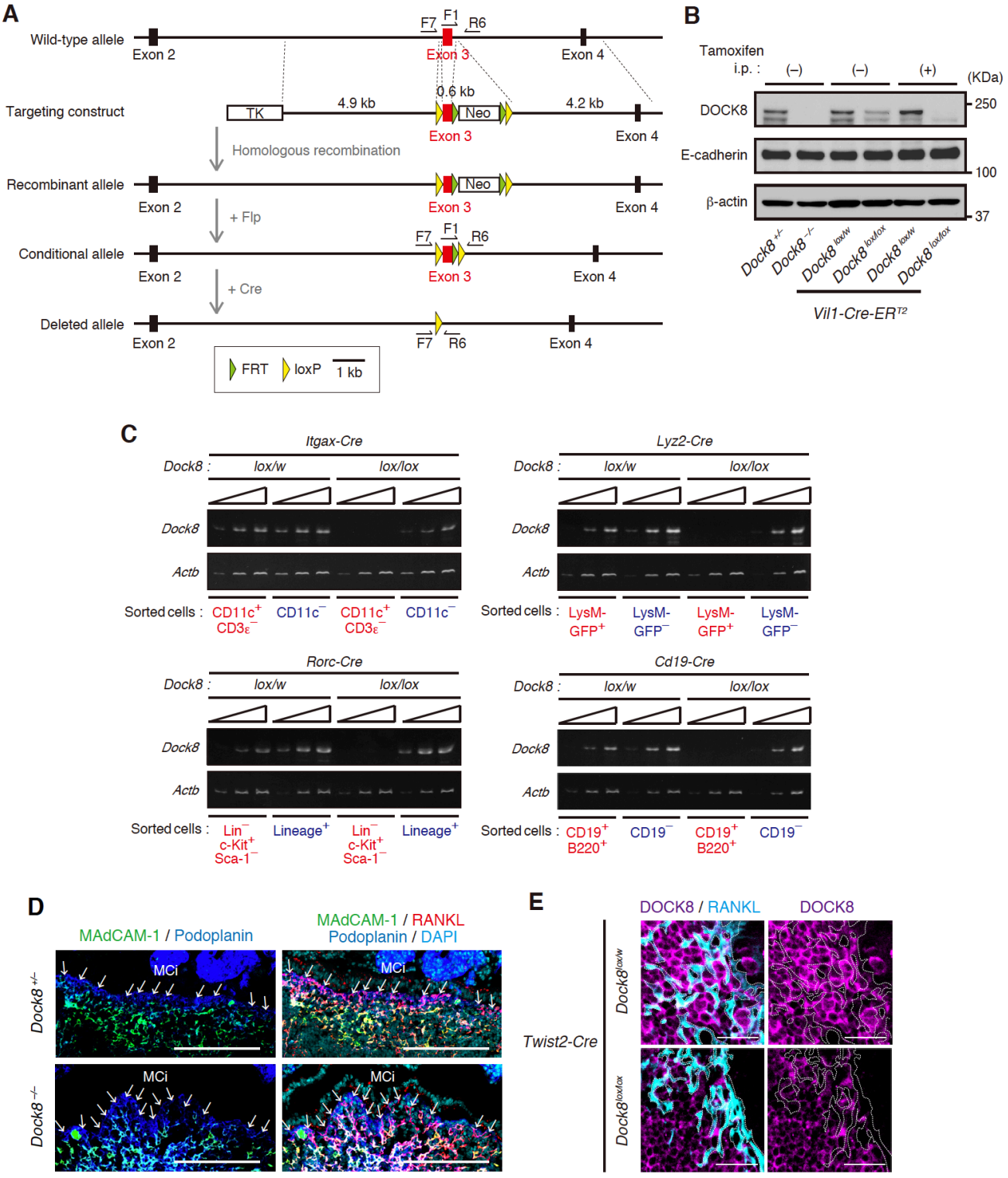

Figure S2. Generation and validation of *Dock8*$^{lox/lox}$ mice. Related to Figure 2.

(A) *Dock8*$^{lox/lox}$ mice have been developed by homologous recombination in embryonic stem (ES) cells.

(B) Representative immunoblot showing DOCK8 expression in intestinal epithelial cells from *Vil1-Cre-ER*^{T2} *Dock8*$^{lox/lox}$ and *Dock8*$^{lox/w}$ mice with or without tamoxifen treatment. As controls, samples from *Dock8*$^{+/-}$ and *Dock8*$^{-/-}$ mice were also included.

(C) Reverse transcription-PCR analysis for the expression of *Dock8* and *Actb*. The specified cells were sorted from PPs of *Dock8*$^{lox/w}$ and *Dock8*$^{lox/lox}$ mice that had been crossed with the indicated cell-type specific *Cre* mice. In

some experiments, LysM-GFP mice were also used. Amplification increased by 3 cycles, from the left to the right, starting at 24 cycles for *Actb* or 30 cycles for *Dock8*.

(D) Immunohistochemical analyses for MAdCAM-1^{-} Podoplanin^{+} RANKL^{+} MCi cells in PPs from *Dock8*$^{+/-}$ and *Dock8*$^{-/-}$ mice. Data are representative of three independent experiments. Scale bars, 100 μm. See the reference (Nagashima et al., 2017) for staining of MCi cells.

(E) Immunohistochemical analyses for the SED area of PPs from *Twist2-Cre Dock8*$^{lox/w}$ and *Dock8*$^{lox/lox}$ mice showing that DOCK8 expression was deleted in RANKL-positive stromal cells. Scale bars, 20 μm.

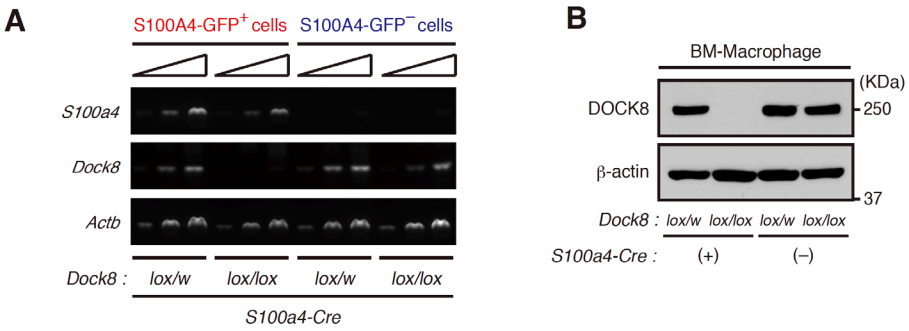

Figure S3. Loss of DOCK8 expression in S100A4-producing cells from *S100a4-Cre Dock8$^{lox/lox}$* mice. Related to Figure 3.

(A) Reverse transcription-PCR analysis for the expression of *S100a4*, *Dock8*, and *Actb* in S100A4-GFP^{+} or S100A4-GFP^{-} cells. Cells were sorted from PPs of *S100a4-Cre Dock8$^{lox/w}$* and *Dock8$^{lox/lox}$* mice expressing S100A4-GFP reporter construct. Amplification increased by 3 cycles, from the left to the right, starting at 24 cycles for *S100a4* and *Actb*, or 30 cycles for *Dock8*.

(B) Representative immunoblot showing DOCK8 expression in BM-derived macrophages from *S100a4-Cre Dock8$^{lox/w}$* and *Dock8$^{lox/lox}$* mice. BM-derived macrophages are known to produce S100A4 protein.

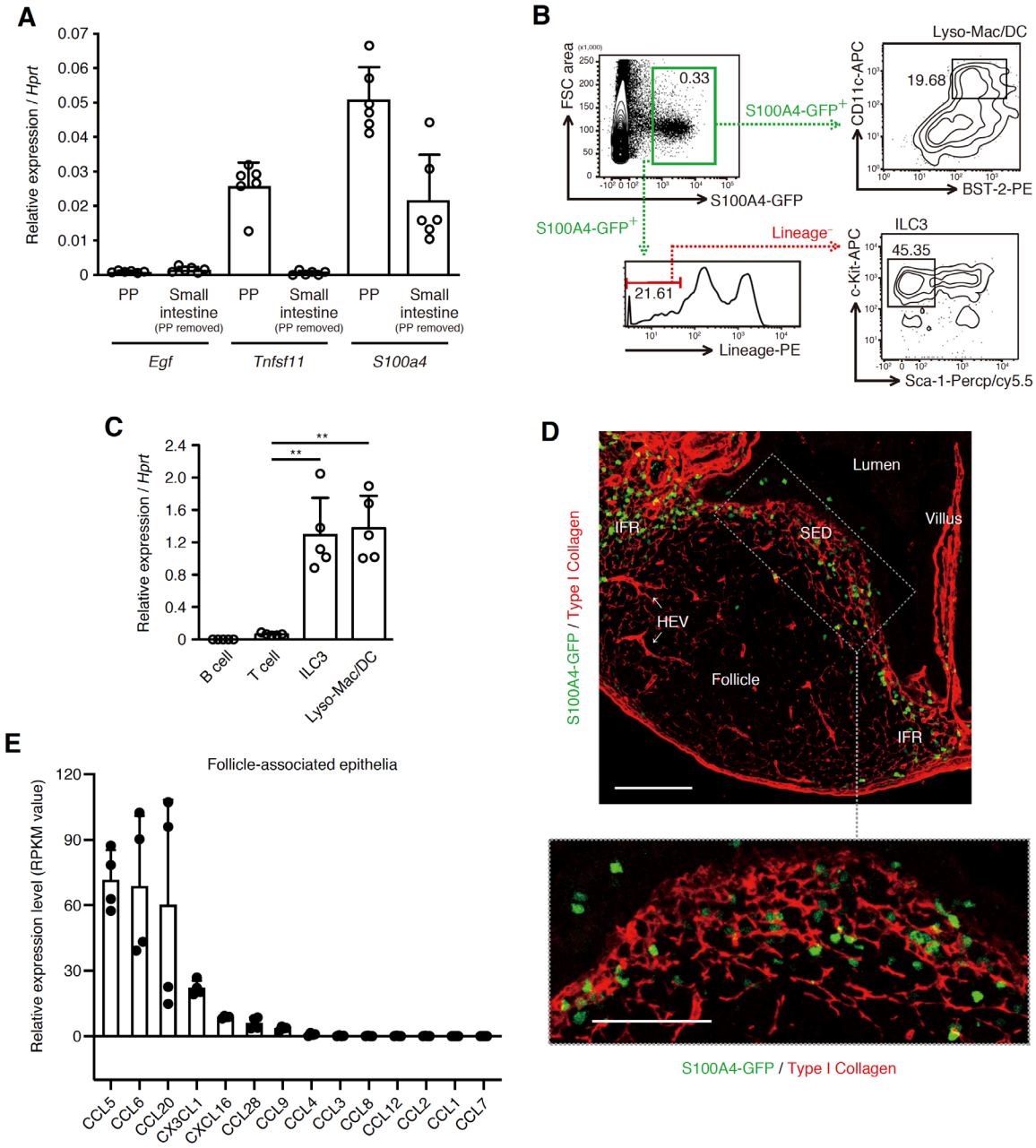

Figure S4. Characterization and localization of S100A4-producing cells in PPs. Related to Figure 4.

(A) PPs and other small intestinal tissues were prepared from WT C57BL/6 mice. Total RNA was extracted with ISOGEN, and *Egf*, *Tnfsf11*, and *S100a4* gene expressions were analyzed by real-time PCR. *Tnfsf11* encodes RANKL. Data (n = 6) were normalized with *Hprt* expression.

(B) The gating strategy used to identify Lyso-Mac/DC and ILC3 cells in S100A4-GFP mice. Cells were isolated from PPs of S100A4-GFP mice and stained for CD11c, BST-2, c-kit and Sca1. To identify ILC3 cells, the following lineage markers were used: B220, CD3ε, CD8α, CD11b, CD11c, Gr1 (Ly6G/Ly6C), NK1.1, and FcεR1.

(C) Real-time PCR analyses for *S100a4* gene expression in CD19$^+$ B220$^+$ B cells, CD3ε$^+$ CD4$^+$ T cells, RORγt-GFP$^+$ c-kit$^+$ Sca1$^-$ lineage$^-$ ILC3 cells and lysozyme-M-GFP$^+$ CD11c^{high} BST2$^+$ Lyso-Mac/DC cells. Data (n = 5) were normalized with *Hprt* expression, and are expressed as mean ± SD. $^{**}P < 0.01$ by two-tailed unpaired Student's *t*-test.

(D) The SED area is rich in collagen fibers. Immunohistochemical analyses for PPs from S100A4-GFP mice. Tissue sections were stained for type 1 collagen. Higher magnification (lower panel) of the area is outlined at upper

panel. Scale bars, 300 μm (upper) and 200 μm (lower). Data are representative of three independent experiments.

(E) Chemokine expression levels in the FAE of PPs from *Tnfrsf11a*$^{f/\Delta}$ mice (n = 4). The figure was generated from the RNA-seq data (GSE93319 in Nagashima et al., 2017).

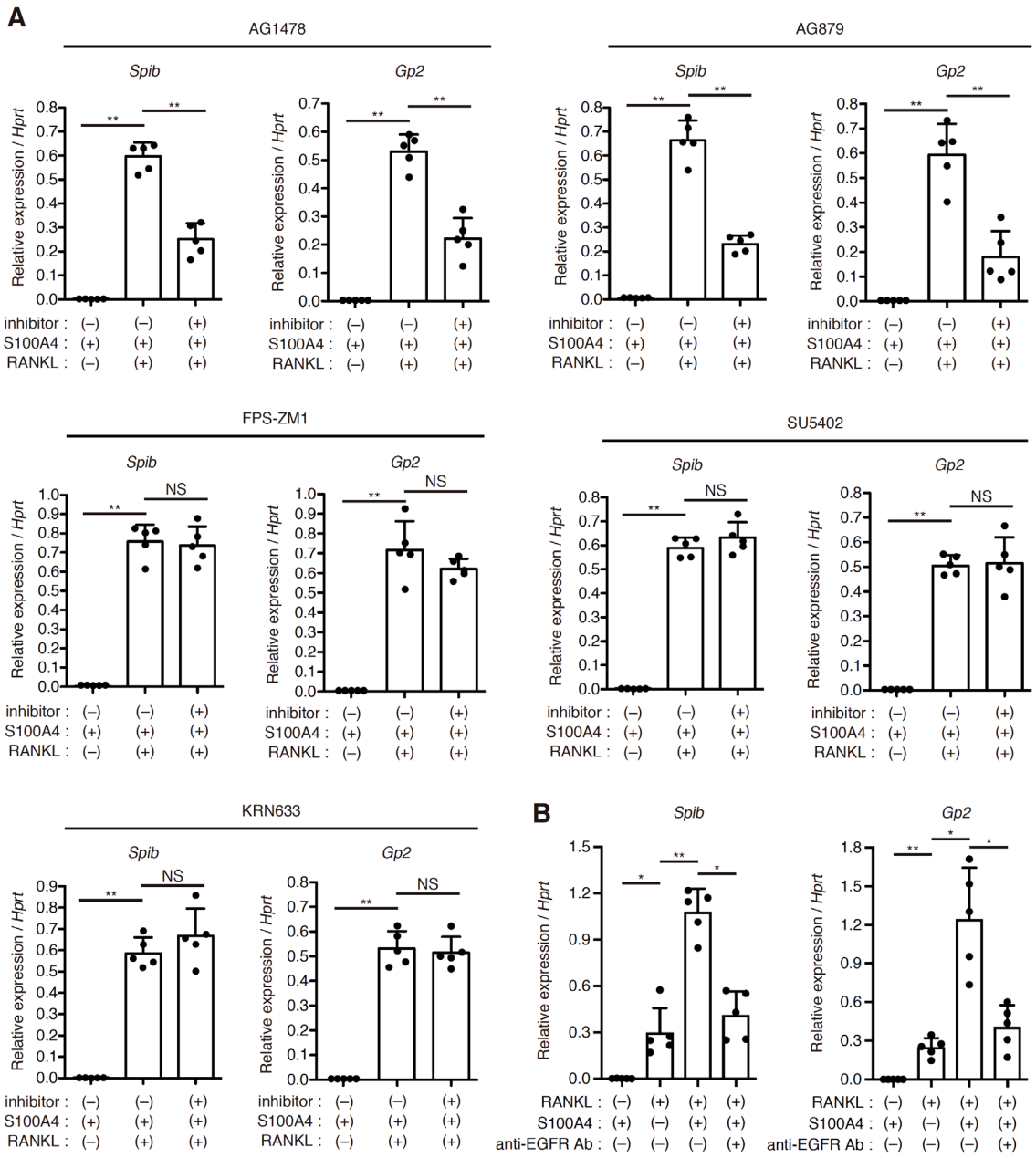

Figure S5. Effect of inhibitors and anti-EGFR antibody on *Spib* and *Gp2* expression in organoids. Related to Figure 5.

(A) Expression of *Spib* and *Gp2* in the organoids generated from WT mice in the presence of RANKL, S100A4 and/or tyrosine kinase inhibitors. The following inhibitors were used: AG1478 for ErbB1 (300 nM), AG879 for Erb2 and TrkA (5 μM), FPS-ZM1 for RAGE (10 μM), SU5402 for FGFR1, VEGFR2, and PDGFR (10 μM), KRN633 for VEGFR1 and VEGFR3 (1 μM). Data (n = 5) were normalized with *Hprt* expression, and are expressed as mean ± SD. $^{**}P < 0.01$; NS, not significant by one-way ANOVA with Tukey's multiple-comparison test.

(B) Expression of *Spib* and *Gp2* in the organoids generated from WT mice in the presence of RANKL, S100A4 and/or anti-EGFR neutralizing antibody. Data (n = 5) were normalized with *Hprt* expression, and are expressed as mean ± SD. $^{*}P < 0.05$; $^{**}P < 0.01$ by one-way ANOVA with Tukey's multiple-comparison test.

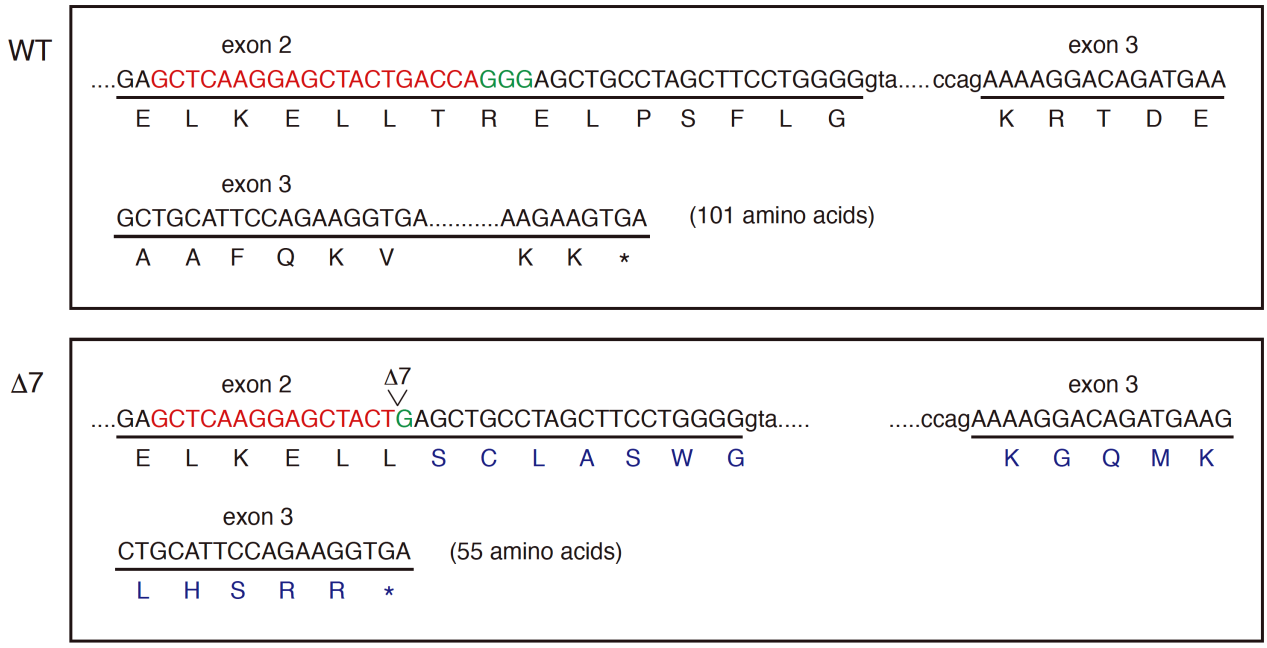

Figure S6. Generation of *S100a4*$^{-/-}$ mice by using the CRISPR/Cas9 system. Related to Figure 6.

Genomic sequence of the mutant allele and the deduced amino acid sequence based on the transcript are shown. The guide RNA for genome editing by CRISPR/Cas9 system was designed within the exon 2. Guide sequence (red), PAM (green) and position of nucleotide deletion (Δ7) are indicated. This deletion leads to frame-shift in the last amino acid sequence encoded by exon 2, and results in a premature stop codon in exon 3.

Table S1. List of primers used in this study (Related to STAR Methods)

Gene	Forward Sequence (5'- 3')	Reverse Sequence (5'- 3')
Conventional RT-PCR		
S100a4	TCAGGCAAAGAGGGTGACAAG	TGCGAAGAAGCCAGAGTAAGG
Dock8	AGTGGACTTTGAAGGACTCGTG	TCCGGTTTACAATCAGCCACTC
Actb	TGGAATCCTGTGGCATCCATGAAAC	TAAAACGCAGCTCAGTAACAGTCCG
Real-time PCR		
Gp2	CTGCGTTCTGACACTGGTATCTC	GATTCTGGCAGGGATCAAAGC
Spib	AGCGCATGACGTATCAGAAGC	GGAATCCTATACACGGCACAGG
Ccl9	GCCCAGATCACACATGCAAC	AGGACAGGCAGCAATCTGAA
Tnfaip2	GTGCAGAACCTCTACCCCAATG	TGGAGAATGTCGATGGCCA
Marcksl1	GGTGATTCCTCAGCCTCCTC	CTCCTCTTCTGTGTCTCCTTCCTT
Anxa5	TCGCCACCTCCCTGTATTCT	GCGGGACACTGCTTTCATC
Tnfsf11	CAGCATCGCTCTGTTCCTGTA	CTGCGTTTTCATGGAGTCTCA
Sox8	TCCGTTGCTCTCCGGTTT	GCCCATTCTCTCCTTTGTCCT
Egf	GACTGAGTTGCCCTGACTCTAC	TGGGCATCCTGGATAACTATTTCG
S100a4	GAGCAACTTGGACAGCAACAG	TTATCTGGGCAGCCCTCAAAG
Hprt	CTGGTGAAAAGGACCTCTCG	TGAAGTACTCATTATAGTCAAGGGCA